AFOSR-TR- 88-1003

(2)

NorthWest Research Associates, Inc.
P.O. Box 3027 • Bellevue, WA 98009

NWRA-CR-88-R029

STUDIES OF INTERNAL WAVE/MEAN FLOW INTERACTIONS

Donald P. Delisi

Northwest Research Associates, Inc.
P.O. Box 3027
Bellevue, WA 98009

27 June 1988

FINAL REPORT FOR THE PERIOD 1 NOV 1986 THRU 30 APR 88

Prepared for

AIR FORCE OFFICE OF SCIENTIFIC RESEARCH
Building 410
Bolling AFB, DC 20332-6448

300 - 120th Ave. N.E. • Suite 220, Building 7 • Bellevue, WA 98005 • (206) 453-8141

Unclassified
SECURITY CLASSIFICATION OF THIS PAGE

REPORT DOCUMENTATION PAGE

Form Approved
OMB No. 0704-0188
Exp. Date: Jun 30, 1986

1a. REPORT SECURITY CLASSIFICATION Unclassified	1b. RESTRICTIVE MARKINGS
2a. SECURITY CLASSIFICATION AUTHORITY	3. DISTRIBUTION/AVAILABILITY OF REPORT APPROVED FOR PUBLIC RELEASE; DISTRIBUTION UNLIMITED
2b. DECLASSIFICATION/DOWNGRADING SCHEDULE	
4. PERFORMING ORGANIZATION REPORT NUMBER(S) NWRA-CR-88-R029	5. MONITORING ORGANIZATION REPORT NUMBER(S) AFOSR-TR- 88-1003
6a. NAME OF PERFORMING ORGANIZATION Northwest Research Associates, Inc. 6b. OFFICE SYMBOL (If applicable) CR	7a. NAME OF MONITORING ORGANIZATION Air Force Office of Scientific Research
6c. ADDRESS (City, State, and ZIP Code) 300 120th Ave. NE, Bldg. 7, Suite 220 P.O. Box 3027 Bellevue, WA 98009	7b. ADDRESS (City, State, and ZIP Code) Building 410 Bolling AFB, DC 20332-6448
8a. NAME OF FUNDING/SPONSORING ORGANIZATION Air Force Office of Scientific Research 8b. OFFICE SYMBOL (If applicable) AFOSR	9. PROCUREMENT INSTRUMENT IDENTIFICATION NUMBER F49620-86-C-0015
8c. ADDRESS (City, State, and ZIP Code) Bldg 410 Bolling AFB DC 20332-6448	10. SOURCE OF FUNDING NUMBERS PROGRAM ELEMENT NO. 61102F; PROJECT NO. 3005; TASK NO. A1; WORK UNIT ACCESSION NO.

11. TITLE (Include Security Classification)

Studies of Internal Wave/Mean Flow Interactions

12. PERSONAL AUTHOR(S)

Donald P. Delisi

13a. TYPE OF REPORT	13b. TIME COVERED	14. DATE OF REPORT (Year, Month, Day)	15. PAGE COUNT
FINAL	FROM 861101 TO 880430	88 June 27	51

16. SUPPLEMENTARY NOTATION

17. COSATI CODES			18. SUBJECT TERMS (Continue on reverse if necessary and identify by block number)
FIELD	GROUP	SUB-GROUP	
			internal gravity waves; mean flow; shear interactions

19. ABSTRACT (Continue on reverse if necessary and identify by block number)

A laboratory facility to observe internal gravity wave/mean flow interactions is described, and results from experiments are presented. The laboratory measurements include density measurements, instantaneous and mean velocity measurements, and shadowgraph observations. The results show that early wavebreaking in turbulent critical layers is characterized by Kelvin-Helmholtz instability and is not convective, as reported in earlier studies. The vertical location of the early overturning moves progressively toward the gravity wave source and is correlated with observed mean flow modifications. Late-time gravity wave/critical layer interactions are characterized by steady-state mixing regions which are phase-locked to the incoming gravity waves. Results from numerical simulations are also presented and are qualitatively similar to the early-time laboratory measurements.

20. DISTRIBUTION/AVAILABILITY OF ABSTRACT ☒ UNCLASSIFIED/UNLIMITED ☐ SAME AS RPT. ☐ DTIC USERS	21. ABSTRACT SECURITY CLASSIFICATION Unclassified
22a. NAME OF RESPONSIBLE INDIVIDUAL Lt Col James p. Koermer	22b. TELEPHONE (Include Area Code) (202) 767-4960 22c. OFFICE SYMBOL NC

DD FORM 1473, 84 MAR 83 APR edition may be used until exhausted. All other editions are obsolete.

SECURITY CLASSIFICATION OF THIS PAGE
Unclassified

NWRA-CR-88-R029

STUDIES OF INTERNAL WAVE/MEAN FLOW INTERACTIONS

Donald P. Delisi

Northwest Research Associates, Inc.
P.O. Box 3027
Bellevue, WA 98009

27 June 1988

FINAL REPORT FOR THE PERIOD 1 NOV 1986 THRU 30 APR 88

Prepared for

AIR FORCE OFFICE OF SCIENTIFIC RESEARCH
Building 410
Bolling AFB, DC 20332-6448

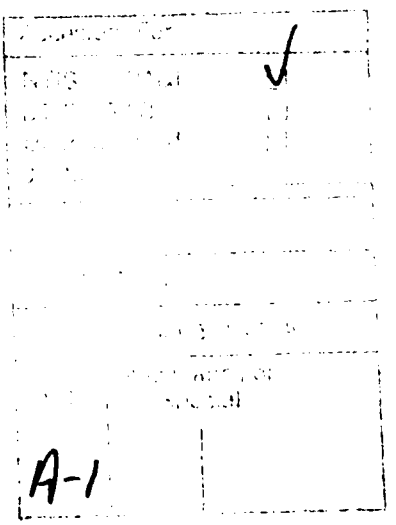

TABLE OF CONTENTS

1. Introduction, Objectives, and Summary of Results

Gravity waves are important in atmospheric circulation because of their ability to transport momentum vertically and to mix tracers and photochemical species. Unstable breakdown of gravity waves in the atmosphere occurs as a wave approaches its critical level (where the mean flow equals the horizontal phase speed of the wave) and by the reduction of density with height (Fritts, 1984).

It is important to understand how gravity waves propagate and eventually dissipate in the atmosphere to be able to predict atmospheric circulation. There are many interactions and couplings between large-scale and small-scale atmospheric phenomena. Many of these couplings and interactions are not, at this time, well understood. This lack of understanding explains, in part, our inability to predict atmospheric conditions globally or locally very far in advance. These interactions and couplings need to be better understood in order to increase our ability to provide long-time atmospheric forecasting through General Circulation Models (GCM's).

Although much is known about gravity wave generation, propagation, and breakdown, our understanding is far from complete. For example, it is thought that large-scale equatorially-trapped gravity waves interacting with vertical shear might be responsible for the quasi-biennial oscillation (QBO) and the semiannual oscillation (SAO) in the tropical middle atmosphere (Holton and Lindzen, 1972; Dunkerton, 1979, 1982b). It is also increasingly recognized that gravity waves are essential to the momentum budget of the upper troposphere and lower stratosphere. Yet, GCM's do not reproduce the QBO and do not accurately reproduce the SAO.

Furthermore, it is becomingly increasingly apparent that tropical atmospheric events are an important part of a global dynamical system. A recent study of ours has shown that the

phase of the QBO is correlated with the non-occurrence of major stratospheric warmings in the northern hemisphere winter during January and February (Dunkerton *et al*, 1988). Two other recent studies of ours have discovered a coupling between sudden warmings in the north polar region and the tropical SAO, which results in one cycle of the SAO being markedly stronger than the other (Delisi and Dunkerton, 1988a, 1988b). Thus, the QBO, which is believed to be driven by gravity wave/mean flow interactions, is correlated with the occurrence of major polar stratospheric warmings which themselves are correlated with the tropical SAO. Other global interactions include correlations of the QBO and Antarctic ozone (Garcia and Solomon, 1987).

Linear theory for the interaction of a gravity wave with a critical layer was first developed by Bretherton (1966) and Booker and Bretherton (1967). Subsequent theoretical research has been performed by Benney and Bergeron (1969), Maslowe (1973, 1977), Grimshaw (1975), Fritts (1979, 1982), Brown and Stewartson (1980), Dunkerton (1980, 1981, 1982a), Lindzen (1981), Dunkerton and Fritts (1984), and many others. For reviews, see Fritts (1984), Maslowe (1986), and Andrews, *et al* (1987).

Observationally, it has been difficult to locate and observe gravity wave/critical layer interactions in the atmosphere. To help understand this phenomenon, several researchers have performed gravity wave/critical layer experiments under controlled, laboratory conditions.

There have been five laboratory studies of gravity wave/critical layer interactions reported in the literature (Bretherton *et al*, 1967; Thorpe, 1973, 1981; Koop, 1981; Koop and McGee, 1986). As pioneering as these efforts were, these studies, were, however, by no means complete. First, nearly all of the results in these studies were qual tative and were not quantitative. Second, all of these experimental studies were of short duration (under 15 seconds for Bretherton *et al*, (1967) and Thorpe, (1973, 1981), and less than 2 minutes for Koop (1981) and

Koop and McGee (1986)). Thus, long-time or steady-state critical layers could not be investigated. These short running times were the results of limitations imposed by the experimental facilities.

The objectives of the current study were (a) to design, build and operate an experimental facility to study the short-time and long-time evolution of gravity wave/critical layer interactions and (b) to obtain quantitative measurements of these interactions.

A summary of our results are the following:

a. The facility has been built and is operative,

b. Gravity wave/critical layer interactions have been observed over time periods of several hours,

c. Early overturning in turbulent critical layers is characterized by Kelvin-Helmholtz instability and is not convective overturning, as reported in earlier numerical studies (e.g., Fritts, 1982; Dunkerton and Fritts, 1984) and laboratory studies (Thorpe, 1981; Koop and McGee, 1986),

d. Measurements indicate mean flow modifications for early-time, turbulent, gravity wave/critical layer interactions are qualitatively similar to those predicted by numerical models,

e. The location of the early overturning is correlated with mean flow modifications, and the mixing region moves progressively towards the gravity wave source, and

f. The late-time gravity wave/critical layer interactions are characterized by mixing regions which are not predicted by numerical models.

In the next section, we discuss the experimental facility. Results are presented in Section 3. Papers and presentations resulting from this work are discussed in Section 4; Section 5 contains a brief summarization of the personnel involved in this effort.

2. The Experimental Facility

Appendix A contains a preprint of initial results from this study in a paper to be published in Pure and Applied Geophysics. Included in this paper is a discussion of the facility at the time the paper was written. We will briefly review that discussion here. For additional details, the reader is referred to Appendix A. Subsequent modifications to the facility that are not discussed in Appendix A will be presented below.

The experimental facility is a modification of one developed by Plumb and McEwan (1978) who performed an analog of the equatorial QBO. Their facility consisted of a cylindrical annulus measuring 0.60 m outer diameter, 0.37 m inner diameter, and 0.50 m high which they filled with stratified salt water.

Our experiment was performed in a cylindrical annular tank with an outer diameter of 1.83 m, an inner diameter of 1.22 m and a height of 0.41 m (Figure 1). The bottom of the tank is comprised of a rubber sheet overlaying thirty-two acrylic sheets. The juncture of each pair of acrylic sheets rests on top of a vertical piston which is connected to a stepper motor which is itself connected to a computer. During an experiment, the computer instructs the stepper motors to drive the bottom floor of the tank up and down, thereby generating a wave of prescribed amplitude and phase speed which progresses around the tank. When the tank is filled with stratified salt water, the bottom floor

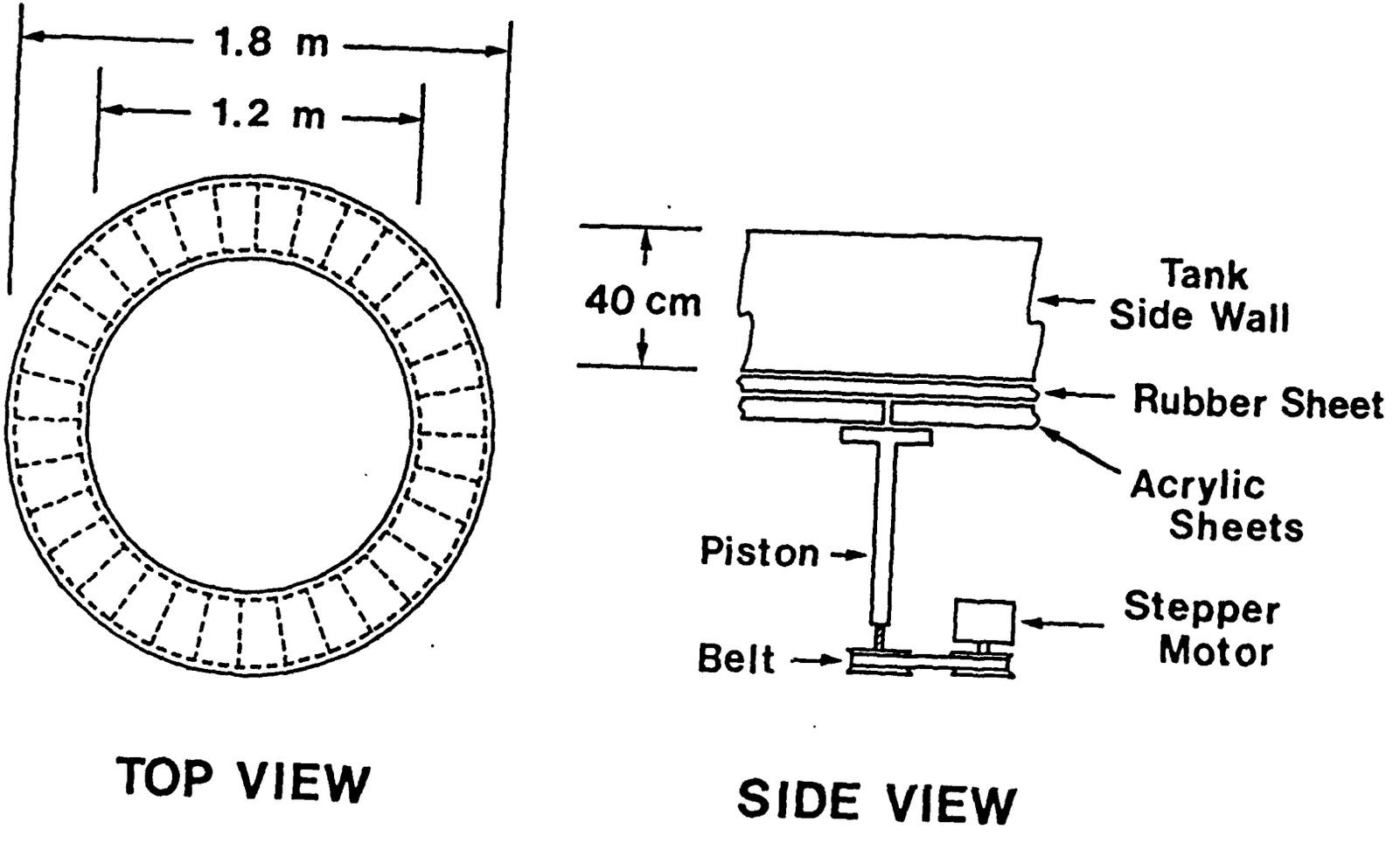

Figure 1. Schematic drawing of the experimental facility.

generates the internal gravity waves which propagate vertically into the fluid.

The wave tank is filled using a standard two-tank storage system (Delisi and Orlanski, 1975). This system generates density profiles which are nearly exactly linear with depth. We have used both two linear density regions (Figure 2) and four linear regions (Figure 2 in Appendix A) in the density profile. The Brunt-Vaisala frequency, N, is defined by

$$N = \left[-\frac{g}{\bar{\rho}} \frac{\partial \rho}{\partial z} \right]^{1/2} \qquad (1)$$

where g is the acceleration due to gravity, ρ is density, $\bar{\rho}$ is average density, and z is the vertical coordinate. In five, two-fluid runs with nominally identical stratifications, N in the top layer was 1.50 ± 0.04 sec^{-1}, and N in the bottom layer was 0.90 ± 0.02 sec^{-1}.

Shear is generated by rotating a lid on the water surface. The lid is an annular acrylic channel which floats on the water surface and is driven by a large O-ring. The lid is adjustable in speed and generates a solid-body velocity profile in the fluid. Early in the study, attempts were made to generate shear by blowing air over the top surface of the water. This blowing technique was eventually discarded because solid-body rotation at the surface was never achieved.

The rotating lid in our facility is a modification of a method used previously in studies of the downward propagation of a mixed region in stratified flows (Kato and Phillips, 1969; Scranton and Lindberg, 1983; Deardorff and Yoon, 1984; and others). These previous investigators used a screen attached to radial arms which were driven from the center of the tank with a rotating shaft. Our technique, we believe, is easier to use and simpler to install than the rotating shaft. In addition, our

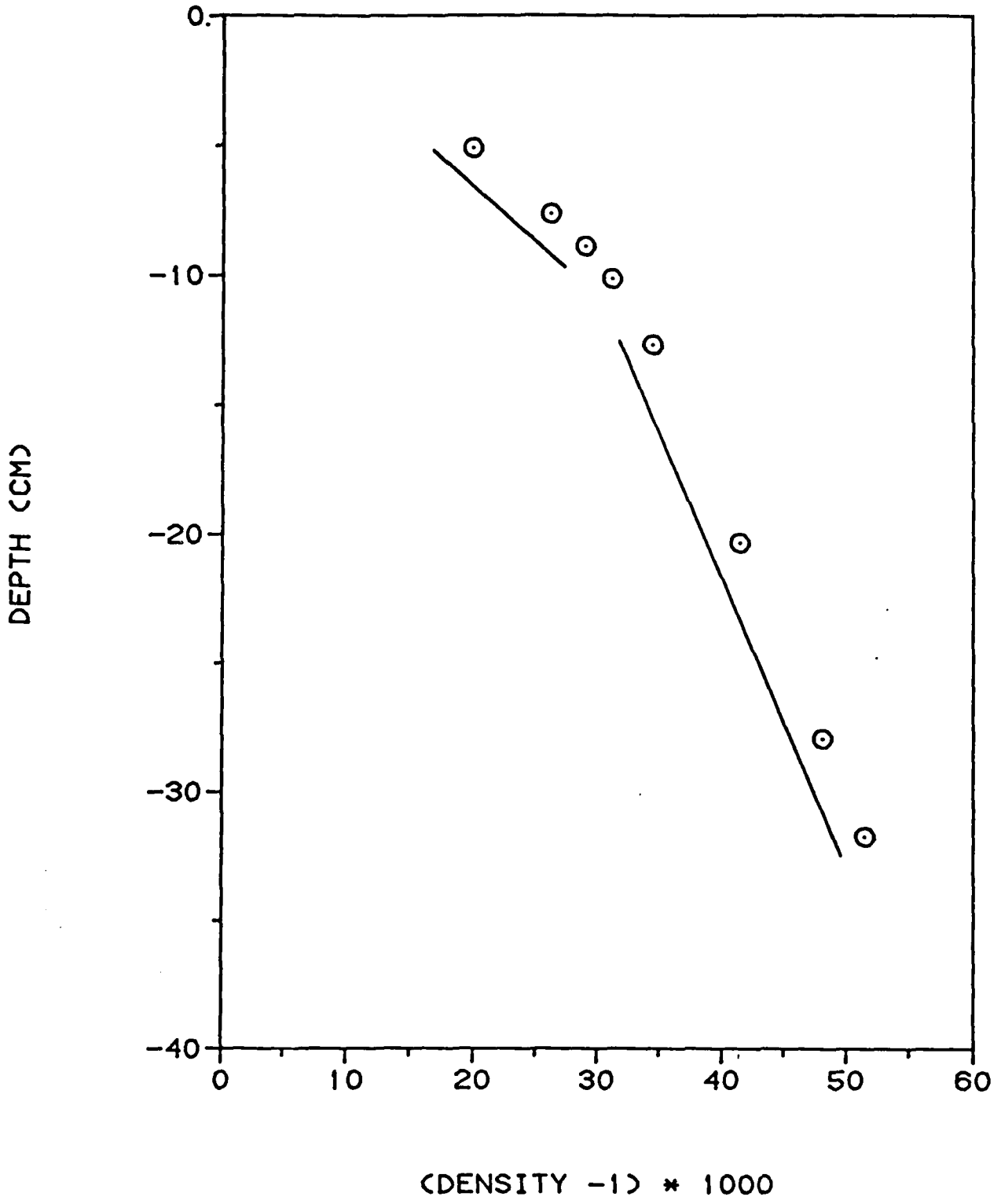

Figure 2. A typical 2-layer density profile. Straight lines are drawn for comparison to linearity.

technique leaves the center of the tank free for the incorporation of a rotating boom (see below).

During an experiment, the rotating lid generates a mixed layer which propagates down into the tank. To minimize the depth of this mixed layer, we placed a high-N region at the top of the tank next to the rotating lid.

The dissipation scale height, d, is given by

$$d \sim \frac{k\hat{c}^4}{\nu N^3} \tag{2}$$

where k is zonal wavenumber, $\hat{c} = c - \bar{U}$, c is the phase speed of the forced wave at the bottom floor, $\bar{U}$ is the mean flow speed, and ν is the kinematic viscosity (Plumb and McEwan, 1978). To minimize wave dissipation and to maximize the wave energy reaching a given vertical level, we want d to be as large as possible. For a given zonal wavenumber and phase speed, then, from eqn. (2), we want N to be as low as possible in the tank. For this reason, we have a lower value of N at the bottom of the tank than at the top of the tank (Figure 2). Earlier experiments used two middle regions of different N to act as transitions between the top and bottom layers. Later experiments used just two layers. No apparent differences were observed between the two-fluid and four-fluid flows.

Flow visualization included a shadowgraph and neutrally buoyant particles. The shadowgraph visualized the second derivative of density. The light source for the shadowgraph was located outside the outer wall of the tank. This allowed easy relocation of the shadowgraph. Shadowgraph images were recorded with a 35-mm camera and a video camcorder.

Neutrally buoyant particles were added to the storage tanks before the filling process was started. Once in the tank, the particles were illuminated using a theatrical spotlight. A 2.5-

cm wide slit at the top of the tank allowed just the particles in a given constant-radius plane to be illuminated. A 35-mm camera was used to record the moving particles. The film in the camera was exposed for 1 or 4 seconds. The resulting streaks in photographic prints were digitized and corrected for parallax to yield instantaneous velocity profiles. Averaging the instantaneous velocity profiles over one cycle of the bottom forcing wave gave the mean velocity profile.

In an experiment, we first filled the tank with a stratified salt solution. We then started the lid, raised the speed of the lid slowly (to minimize the generation of turbulence at the lid and, hence, minimize the depth of the mixed layer) and reached a pre-determined speed of the lid. The speed of the lid was then kept constant until a near-steady state velocity profile was reached. Figure 3 shows several velocity profiles taken at different times after the lid was at constant speed. After the flow was established, internal gravity waves were introduced into the flow by moving the bottom floor of the tank. Wave energy propagated vertically into the tank from the bottom floor, and, if the phase speed of the forced, bottom waves was below the maximum current speed, the waves encountered a critical level. The resulting interactions were then observed. In this study, only monochromatic forcing waves were used, and, once started, the waves were generated continuously throughout the experiment.

The particle motions and shadowgraph visualization were normally observed in the laboratory frame of reference. To allow the observation of the interactions in the incoming wave frame of reference, a rotating boom was constructed. The boom consisted of a variable-speed, rotating shaft at the center of the tank with a horizontal boom connected to the end of the shaft above the tank. The boom extended radially from the center of the tank in both directions and extended in each direction beyond the outer walls of the tank. A platform was constructed at one end of the boom. Slip rings allowed power to be accessible from the platform. Typically, the platform contained the shadowgraph

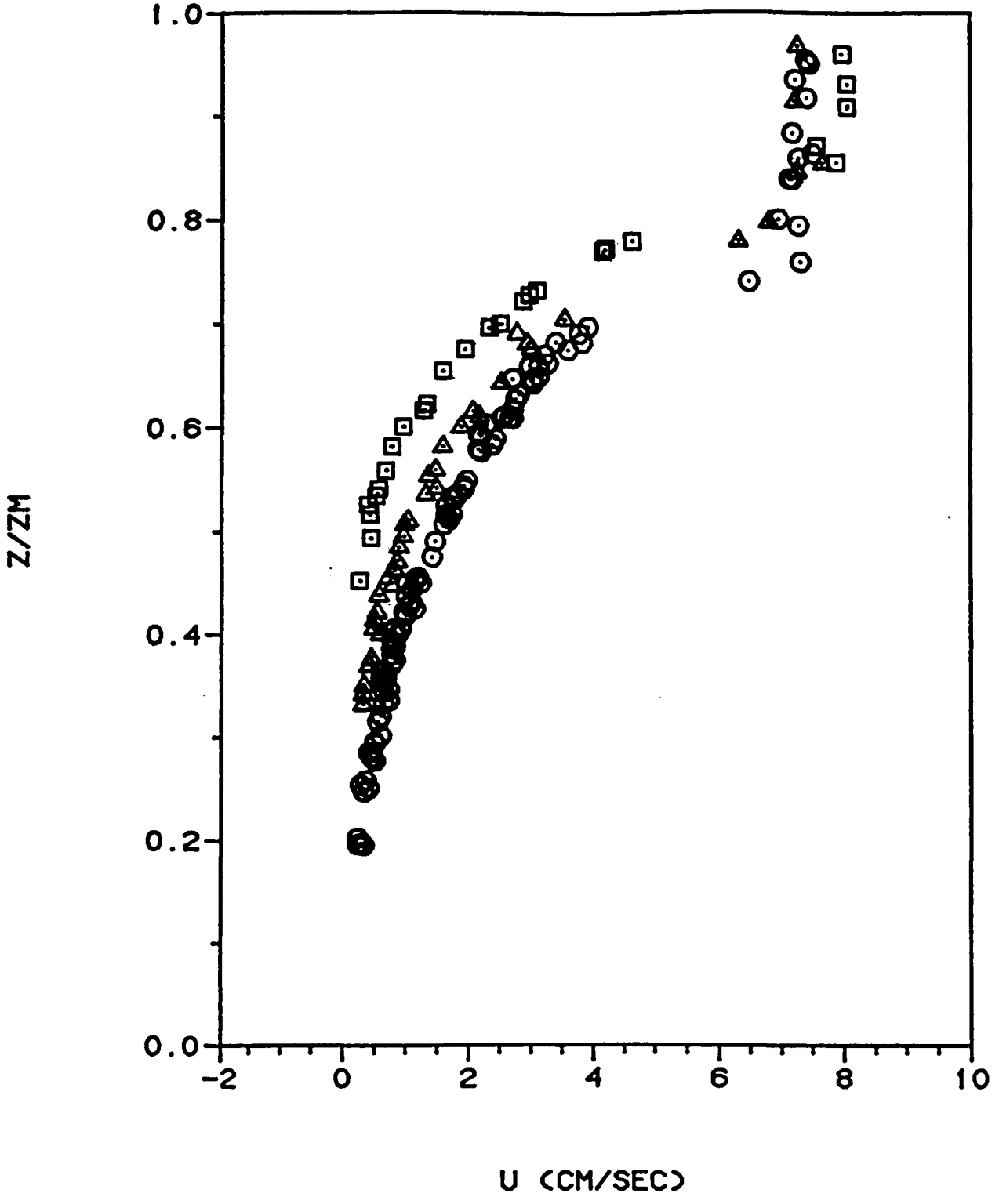

Figure 3. Typical velocity profiles before the run. Squares, triangles, and circles are profiles 15, 45, and 100 minutes after the lid reached full speed. A profile at 75 minutes is identical to the 100-minute profile. The bottom waves start at 105 minutes. Z_M is maximum water depth (38 cm).

light source as well as a 35-mm camera and a video camcorder to record the shadowgraph images. The boom could be adjusted to rotate at any speed but was primarily rotated at the speed of the bottom forcing wave.

To measure density both before and during runs, we used a Seabird Electronics conductivity probe and associated electronics (Microstructure Conductivity Sensor Model SBE-7). The probe was located at the end of a thin rod which penetrated into the side wall of the tank. A right-angle bend in the rod allowed the probe tip to be oriented into the incoming flow. The distance from the right-angle bend to the probe tip was 39.4 cm. The conductivity probe was calibrated before each run with water samples drawn from known depths in the tank. Resulting calibration curves were nearly linear with density (Figure 4).

Two types of conductivity measurements were made. Single depth density measurements were obtained by leaving the conductivity probe at a given depth. To measure density profiles, the conductivity probe was oscillated vertically. Both the speed of rotation and the depth range could be varied. Typically, we rotated over a vertical depth of 18 cm with a period of 20 sec.

The signal from the conductivity probe was recorded on a microcomputer data acquisition system of our design. The frequency of conductivity measurements was under computer control; typically, we recorded 5 samples per second. An incremental encoder signal (BEI Motion Systems E203-512-3) from one drive wheel of the oscillating probe mechanism (to allow us to determine the depth of the probe), a wave crest indicator, and time of day were also recorded with each conductivity measurement.

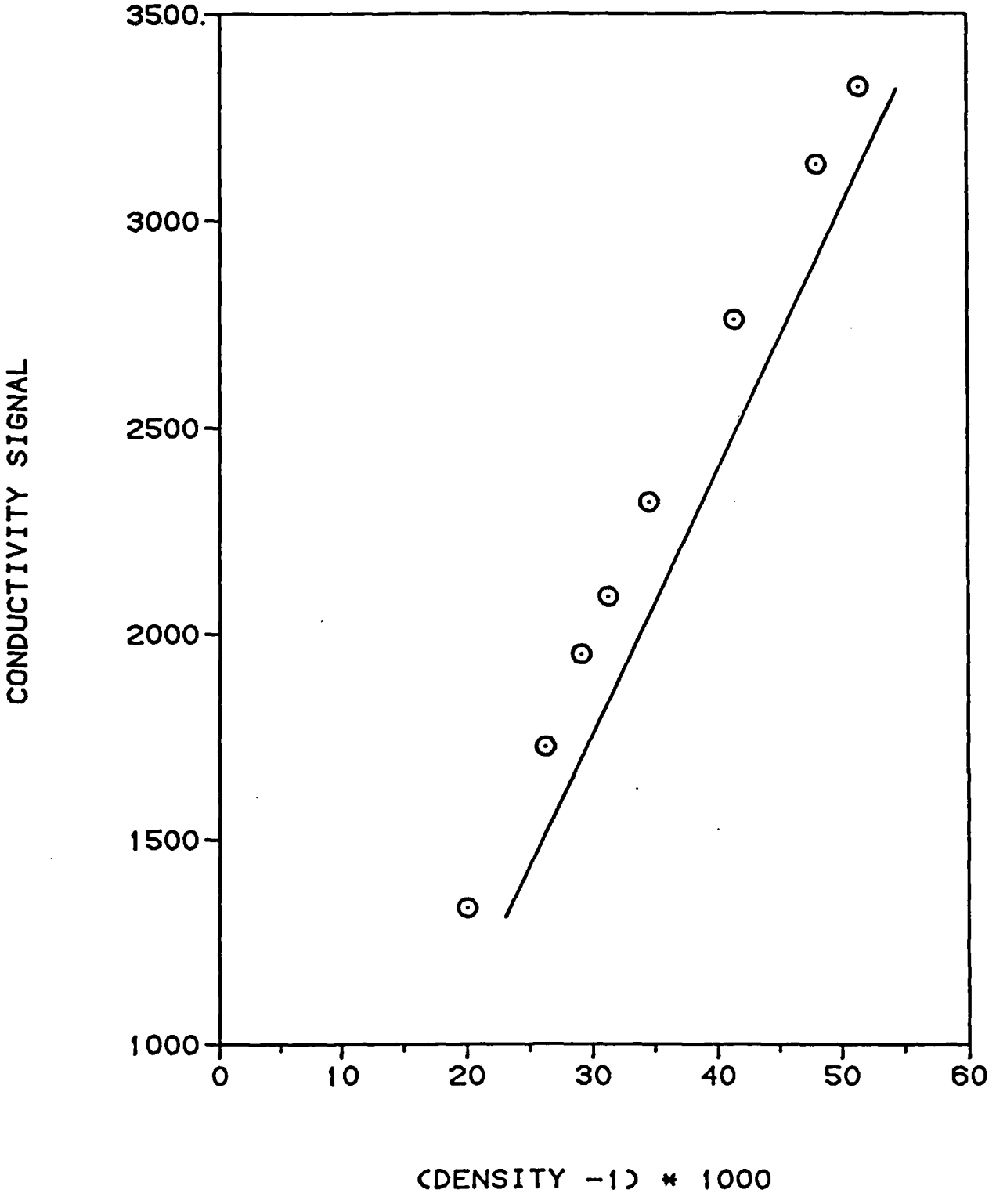

Figure 4. A typical conductivity calibration curve. The straight line is drawn for comparison to linearity.

3. Results

3.1. Laboratory Results

Laboratory results will be presented from three different types of experimental runs:

Case A: the four-fluid case discussed in Appendix A,

Case B: the two-fluid case shown in Figure 2, and

Case C: the two-fluid case shown in Figure 2 with reverse waves.

The experimental parameters for these cases are given below:

Case	Wave-number	Amplitude (cm, pk-to-pk)	Phase Speed (cm/s)	Initial Density Profile	Initial Velocity Profile
A	2	4.0	4.5	Figure 5	Figure 6
B	2	4.0	4.5	Figure 2	Figure 3
C	2	4.0	3.5	Figure 2	Figure 7

For all cases, we used a wavenumber of two, signifying two crests and two troughs for the bottom wave. Amplitudes are in cm, peak-to-peak.

Case A was run twice to determine run-to-run variability. On the other hand, we ran Case B many times to obtain different kinds of data. For example, we positioned the conductivity probe at different vertical locations in several runs. In other runs, we oscillated the probe over different vertical depths. In still other runs, we used a different phase speed of the bottom wave.

In Case C, we started bottom waves going in the direction opposite to the mean flow before the lid was started. These waves continued until 25 minutes before the start of the bottom waves in the direction of the mean flow. We performed this experiment to move the critical layer further from the base of

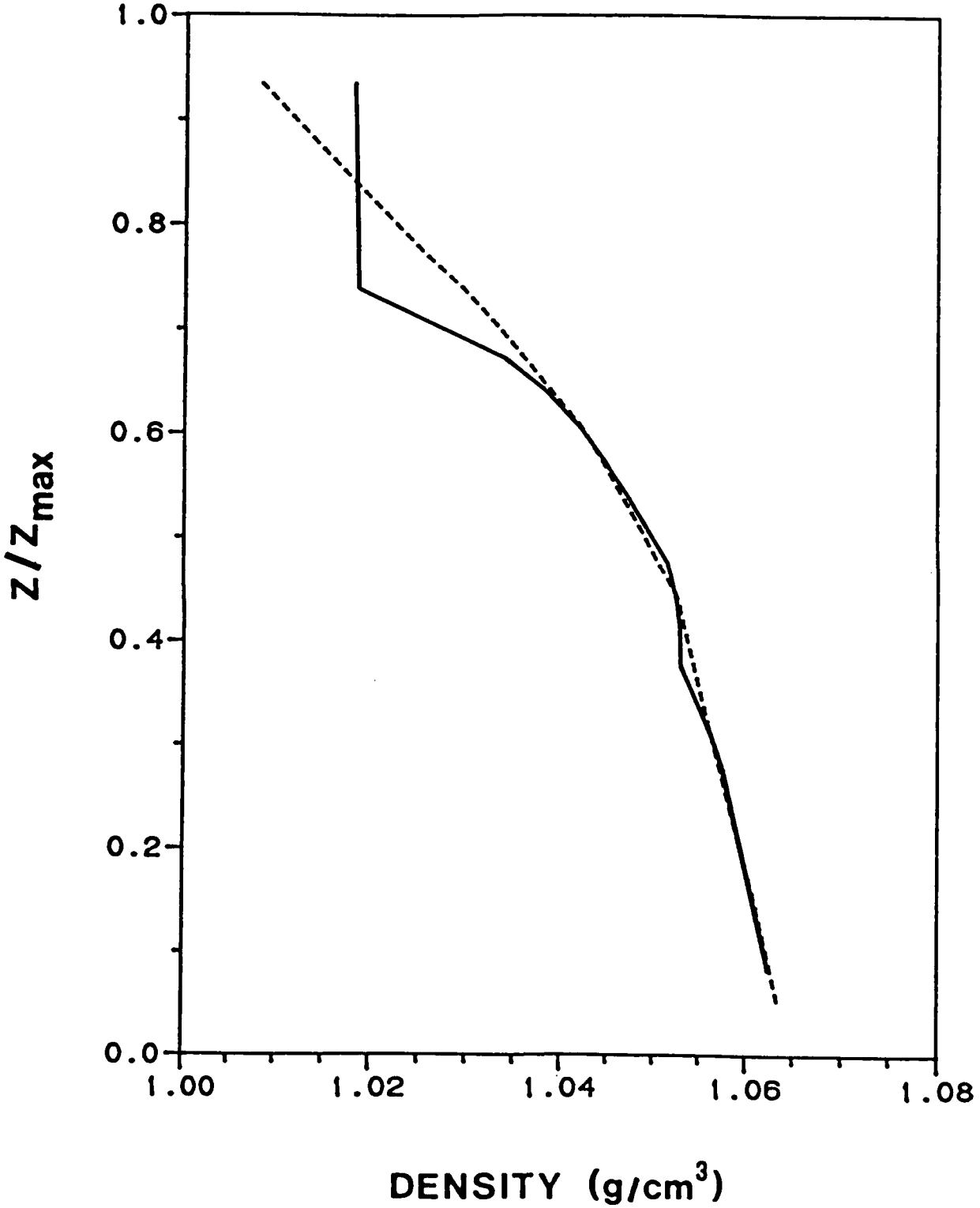

Figure 5. A typical initial (ending) density profile for Case A is the dashed (solid) line.

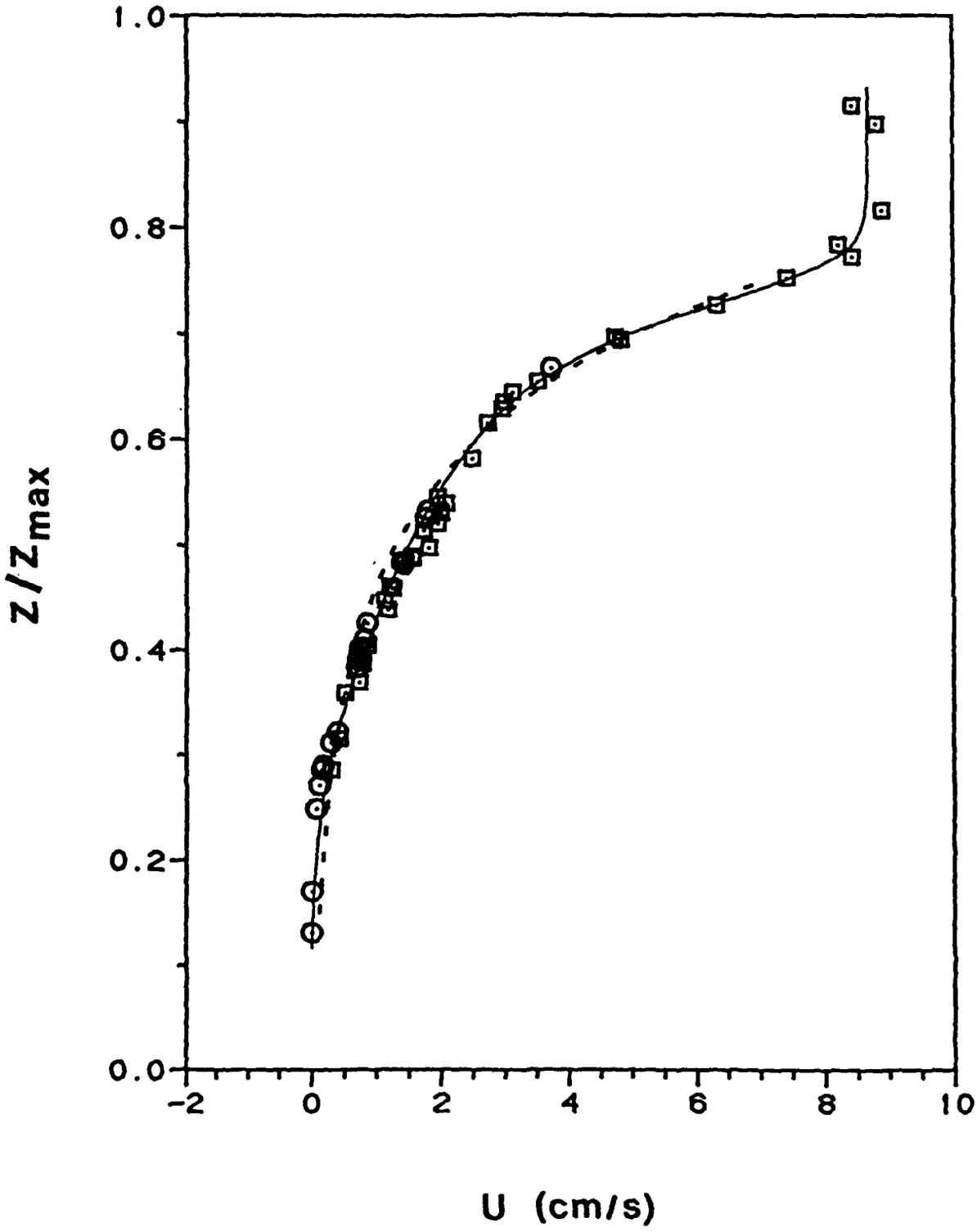

Figure 6. A typical initial velocity profile for Case A. See Appendix A, Figure 3 for additional details.

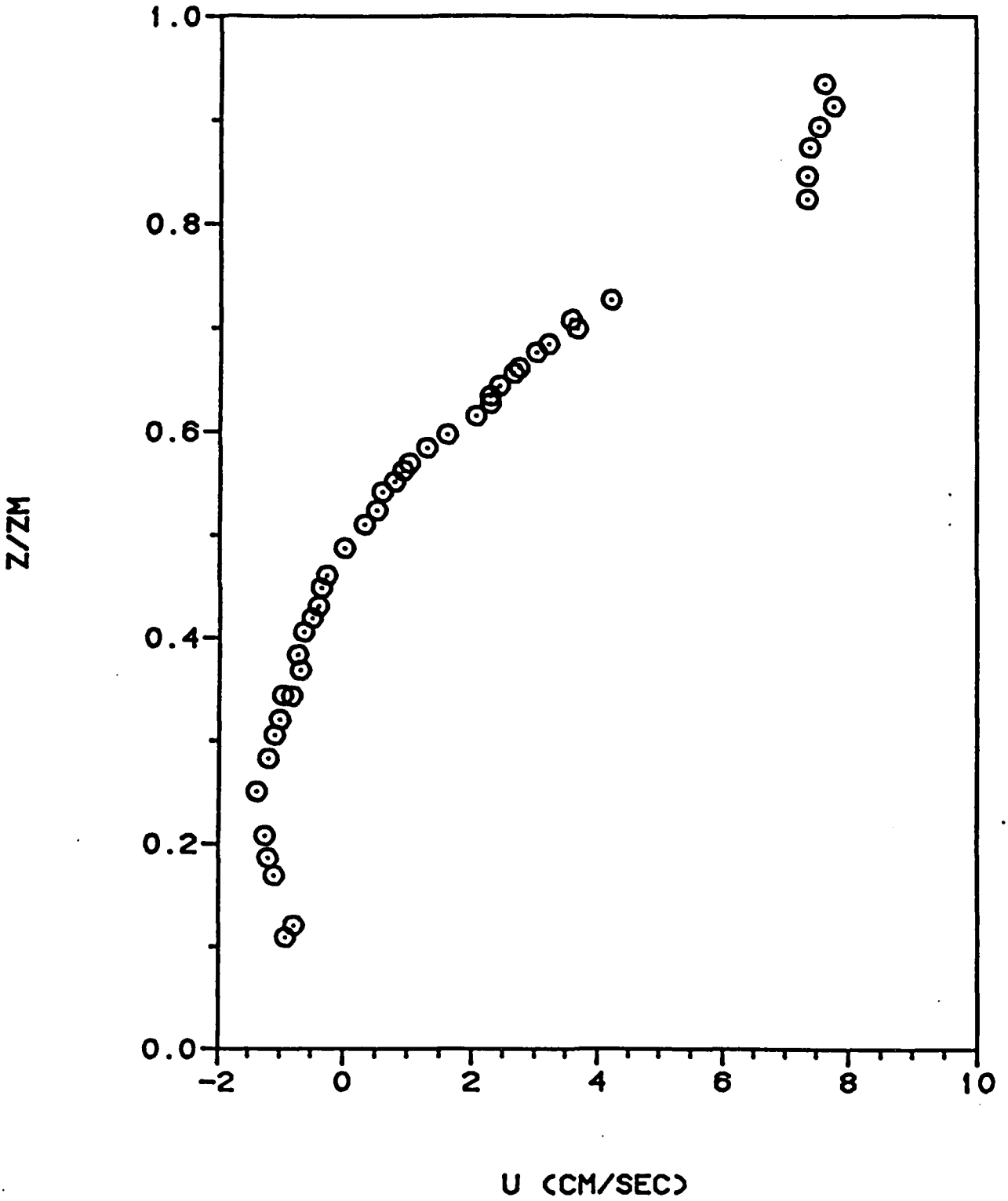

Figure 7. The initial velocity profile for Case C. Z_M is maximum water depth (38 cm).

the mixed layer. Because the reverse waves added a mean flow in a direction opposite that of the bottom, forced waves during the run, $\hat{c}$ in eqn. (2) is approximately equal in Cases B and C even though the phase speeds are different.

Results from all three types of experiments are similar and will be shown interchangeably to stress certain points. When appropriate, we will differentiate between the various runs.

As discussed in Section 2, the instantaneous streak photographs are digitized, corrected for parallax, and plotted to yield instantaneous velocity profiles. An important experimental question is how repeatable this technique is from wave cycle to wave cycle and from run to run (using identical nominal conditions). Figure 8 shows two instantaneous velocity profiles taken at the same phase of the bottom wave from Case C. These two profiles are separated in time by one wave period. There is good agreement between the two profiles, and at least some of the differences between profiles can be attributed to the flow changing slowly with time (see below). Figure 9 shows two profiles from different realizations of Case B. In this figure, the times of the photographs are nearly, but not quite, the same, and, more importantly, the depths of the mixed layers are not exactly the same. Still, there is quite good agreement between the two profiles.

In each gravity wave/critical layer experiment we performed where turbulence was generated, wavebreaking began during the second or third cycle of the bottom wave. The wavebreaking appeared as regions of rolling motions which were inclined in a shallow angle to the horizontal. A schematic drawing of this early wavebreaking is shown in Figure 10 and photographs of the wavebreaking appear in Figure 11. In Figure 10, the dotted rectangular box represents the approximate horizontal and vertical extent of the shadowgraph, and the photographs in Figure 11 show a limited vertical section of that area.

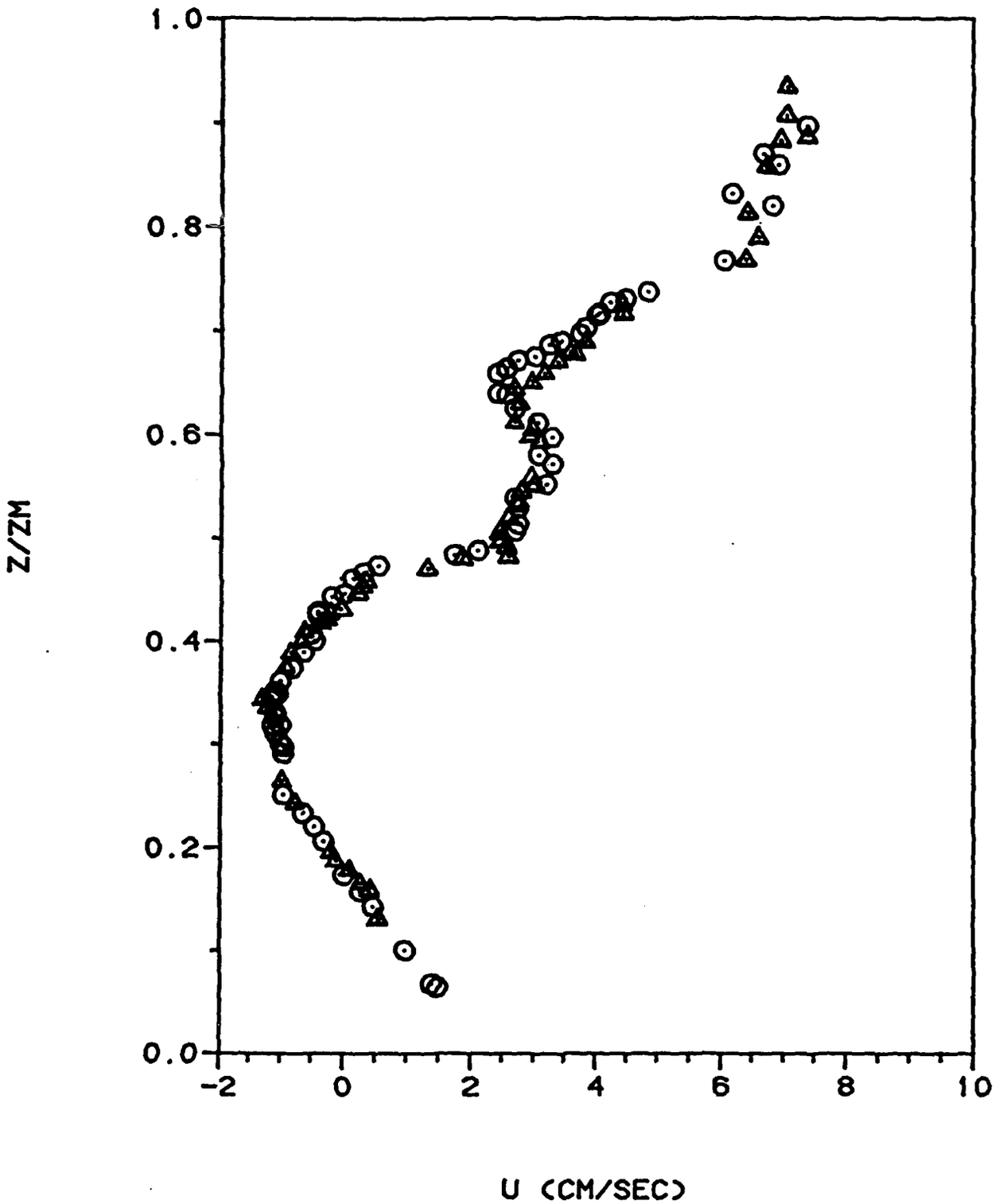

Figure 8. Two instantaneous, particle velocity profiles taken at the same phase of the bottom wave during the same experiment. The circles are data taken 5:54 after the start of the experiment. Triangles are data taken one wave period later.

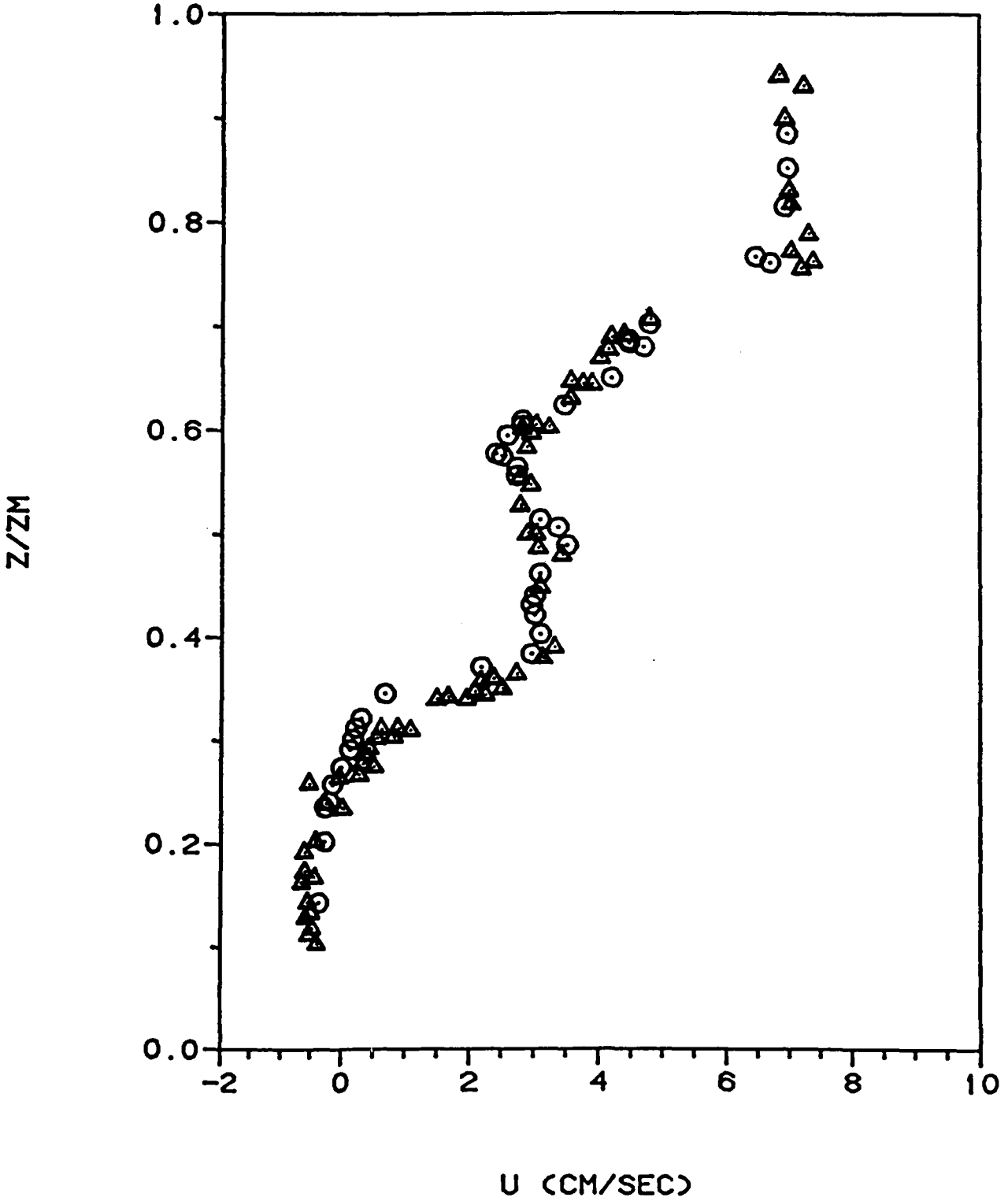

Figure 9. Two instantaneous, particle velocity profiles at nearly the same time (4:55) in different runs for Case B.

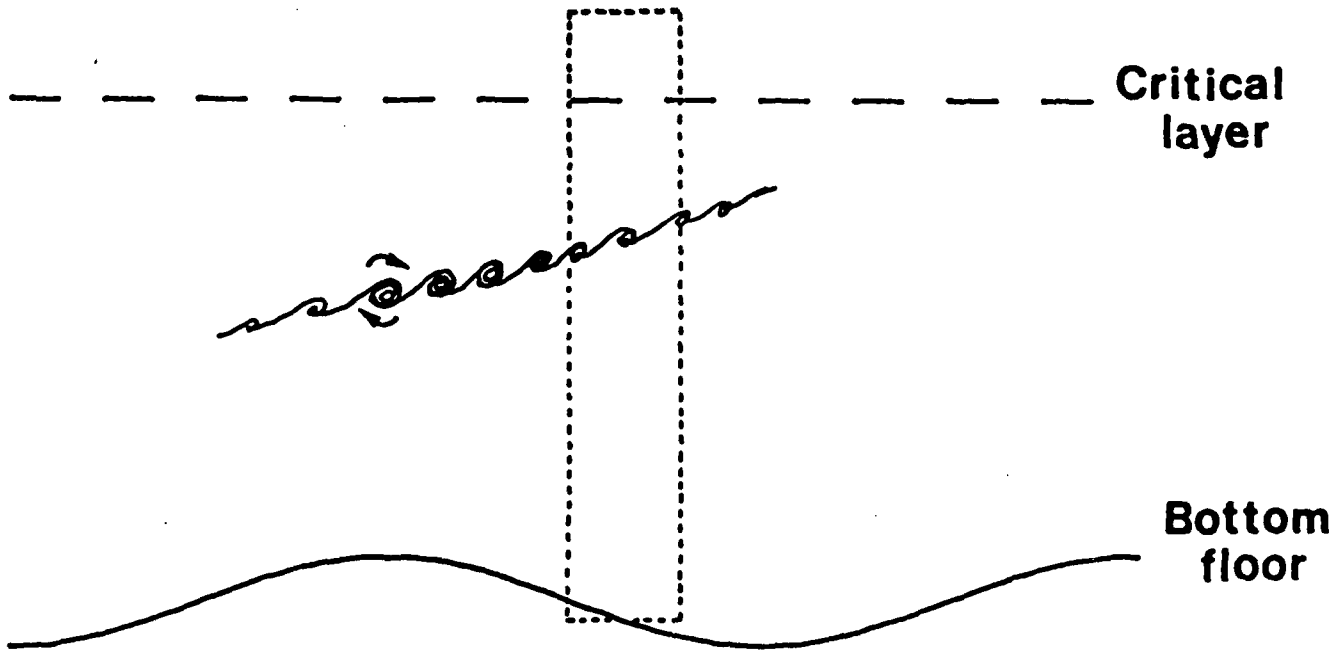

Figure 10. Schematic drawing of early wavebreaking. Arrows indicate the direction of the rolling motions. Flow is from left to right.

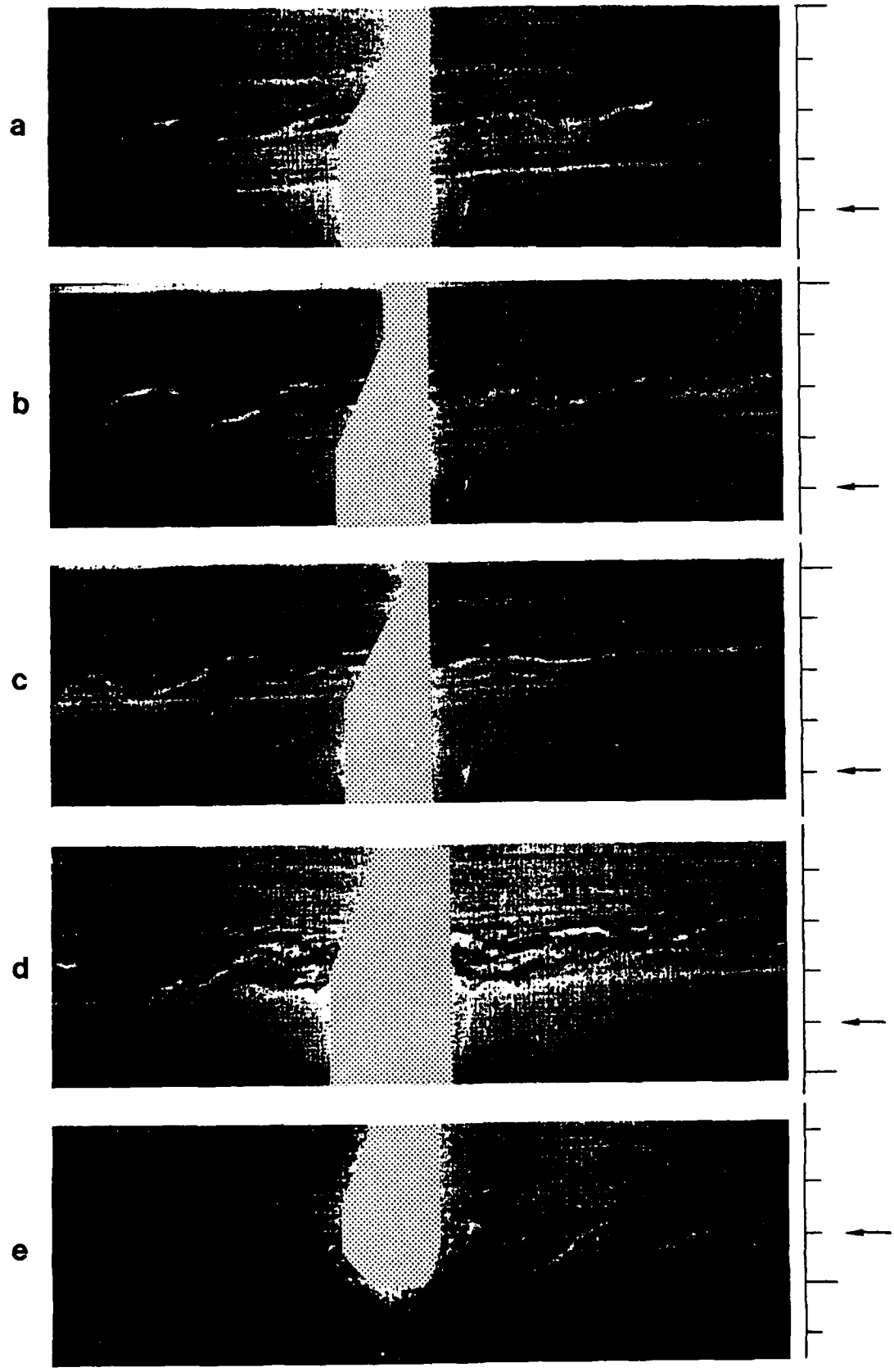

Figure 11. Shadowgraph images of early wavebreaking. See Appendix A, Figure 5 for additional details.

For wavenumber two, the horizontal wavelength of the bottom forcing wave is approximately 240 cm at the centerline of the annulus. Typically, the rolling motions are 10 cm apart, or four percent of the horizontal wavelength.

To characterize the form of the early wavebreaking, we examined the density data from the oscillating conductivity probe and corresponding velocity data from the streak photographs. An example from Case C is given in Figure 12. In Figure 12a, we show contours of constant density from 8 to 24 cm below the lid. The contours are separated by .002 gm/cm^3. These data were obtained from the oscillating conductivity probe. The vertical lines in Figure 12a are located at crests of the bottom wave. For each wave cycle shown, there are approximately 3 1/2 cycles of the probe. Thus, approximately 7 density profiles are used in each wave cycle shown; a total of 23 profiles are used in the figure.

The conductivity data from the probe have been corrected in several ways: First, average data from many up-swings and down-swings of the probe were matched to yield consistent density values. This procedure corrects for the probe dragging heavy fluid up on up-swings and dragging light fluid down on down-swings (Delisi and Kirchhoff, 1977). Second, because the probe oscillates vertically in an arc, we have neglected corrections to the probe trajectory due to horizontal movement of the probe tip. These horizontal movements are approximately 5 cm, or two percent of the horizontal wavelength. Correcting for these horizontal motions would have a negligible effect on the data in Figure 12. Differing times of conductivity measurements have been corrected for in the plots in Figure 12.

The time period shown in Figure 12 is 265 to 475 seconds after the bottom waves are started. Note that time is increasing to the left. This convention is used to make the resulting plot appear as if the flow were from left to right, consistent with Figures 10 and 11.

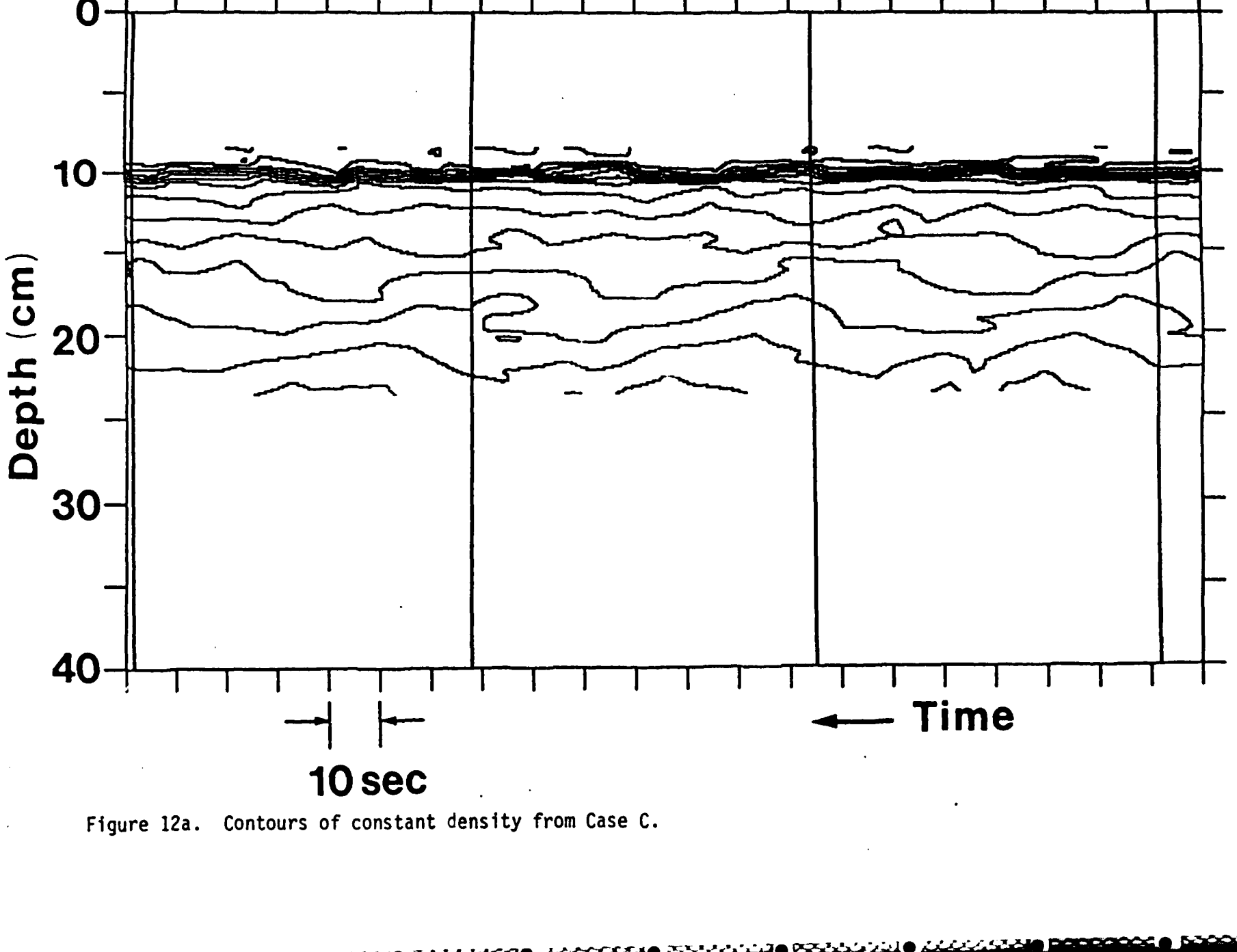

Figure 12a. Contours of constant density from Case C.

In Figure 12a, we see the base of the mixed layer, characterized by a strong density gradient, at the top of plot. Below this strong density gradient is the region of interest. The critical level is several cm below the base of the mixed layer. At a constant depth, for example at a depth of 16 cm, we see a region of strong density gradient around the time of the crest of each bottom wave, followed by a region of weaker density gradient around the time of the trough of each bottom wave.

In Figure 12b, we show the data of Figure 12a on which we have superimposed regions of wavebreaking determined from videos of the shadowgraph. Thus, from observations such as those in Figure 11, we determined the depths of wavebreaking at various times and plotted those depths as the shaded regions in Figure 12b. In this figure, the breaking begins approximately 15 cm below the lid near the trough of the bottom wave and progresses lower in the tank during each wave cycle. The breaking occurs at the base of the weak gradient region in each cycle and just above regions of stronger density gradient.

In Figure 12c, we show Figure 12b superimposed with several, instantaneous velocity profiles. Note several features in this figure. First, in each profile, the maximum, instantaneous velocity shears are located vertically in the regions of wavebreaking. Second, the maximum particle velocities (below the critical level) are located above the regions of wavebreaking and are in the regions of weaker density gradient. Convective overturning will occur when the instantaneous particle speeds exceed the wave phase speed (Orlanski and Bryan, 1969). Hence, convective overturning will occur at vertical locations where the instantaneous particle speeds are a maximum. Here, we see overturning below the maximum particle speeds. Also, the Richardson numbers in the regions of wavebreaking in Figure 12c are between 0.04 and 0.08, which is a range where Kelvin-Helmholtz (K-H) instabilities can occur. Finally, the observed wavebreaking shown in Figure 11 is distinctly reminiscent of K-H instability observed in previous laboratory experiments (Delisi

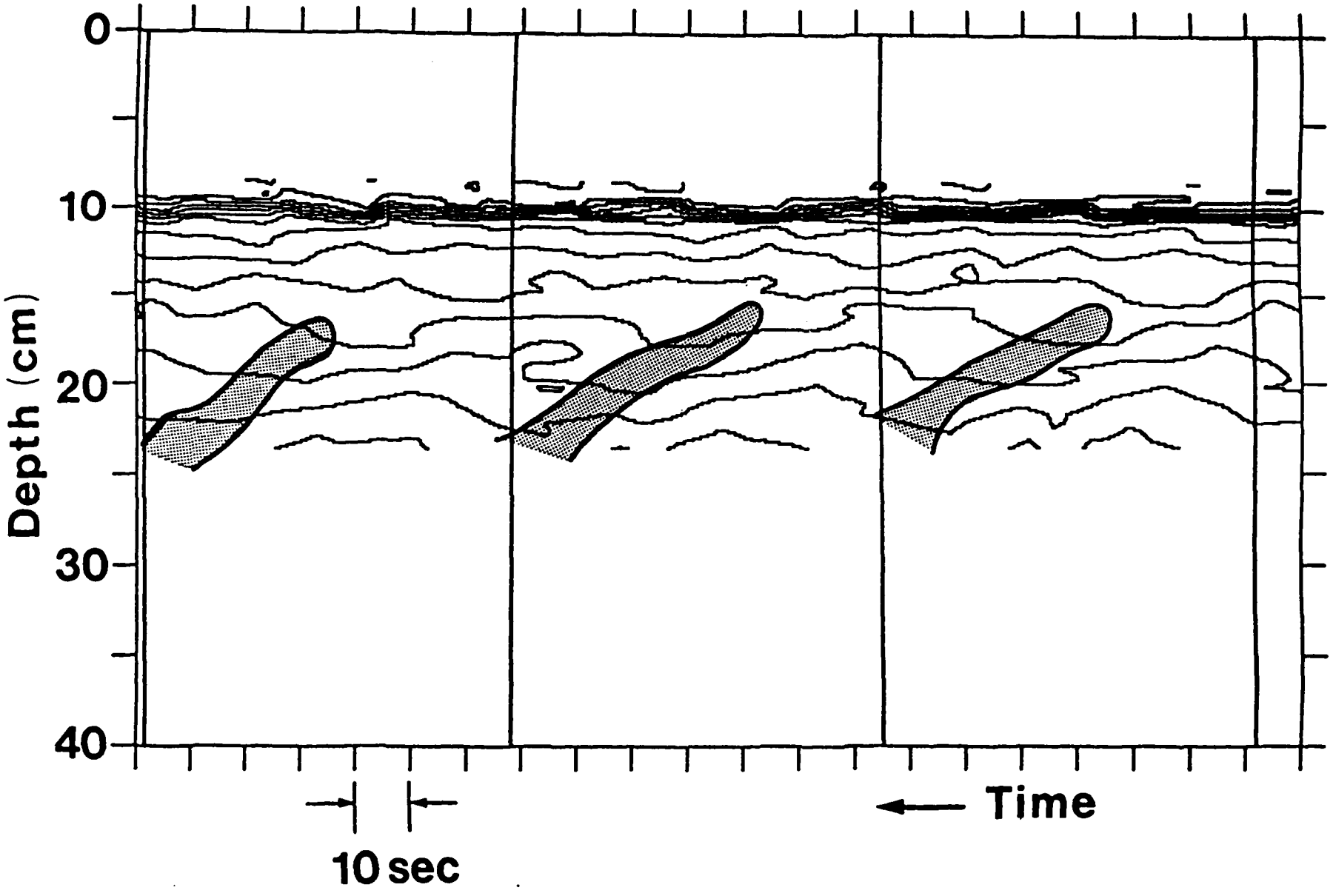

Figure 12b. Figure 12a superimposed with regions of wavebreaking.

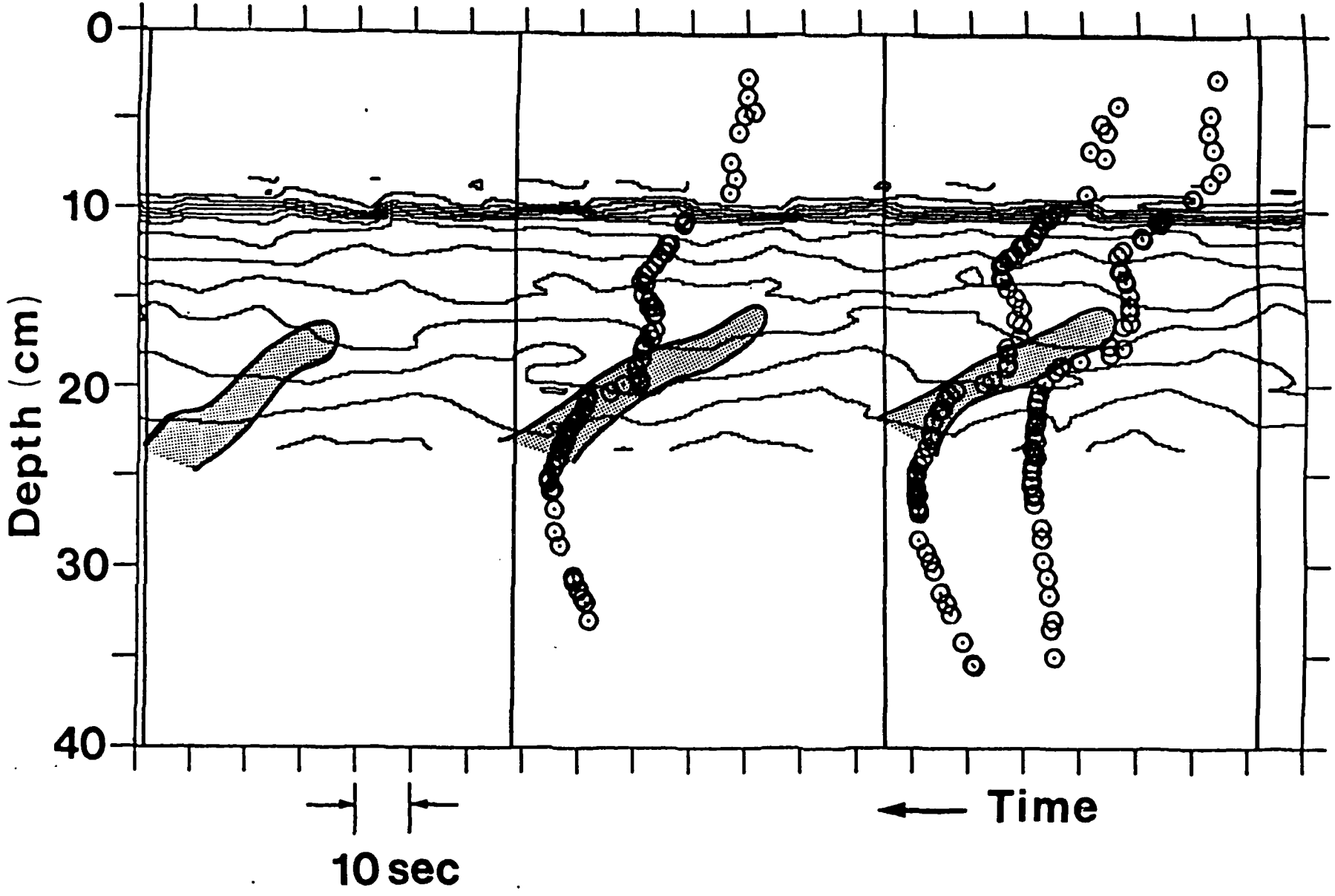

Figure 12c. Figure 12b superimposed with instantaneous particle velocity profiles.

and Corcos, 1973; Thorpe, 1973). Hence, we believe the early wavebreaking observed in our gravity wave/critical layer experiments is Kelvin-Helmholtz and is not convective overturning.

Earlier laboratory results (Thorpe, 1981; Koop and McGee, 1986) and earlier numerical studies (e.g., Fritts, 1982; Dunkerton and Fritts, 1984) reported that the overturning was gravitationally or convectively unstable and not Kelvin-Helmholtz. The reason for the discrepancies between our results and previous studies lies in the scales of the instabilities which are allowed to develop. In Thorpe (1981), the laboratory tank was 16 cm high, and the forcing wave had a horizontal wavelength of 25 or 50 cm. Since the overturning develops below the critical level (which is at mid-depth in his tank), the overturning had to occur in the bottom 8 cm of the tank. Thus, the horizontal and vertical scales of his experiment were limited, and the (shorter) scales of Kelvin-Helmholtz instabilities were viscously damped. Hence, only convective overturning on large scales was allowed to occur. Similarly, with Koop and McGee's (1986) monochromatic wave forcing, the horizontal wavelengths were 7.5 or 15 cm, and the K-H instabilities were viscously damped. Finally, in the numerical studies, too few harmonics were used to allow K-H instabilities to develop. Thus, only in our experiments have K-H instabilities been allowed to develop, and they are observed to be the dominant instability mechanism.

Figure 13 shows data similar to Figure 12 for Case B but for a longer time record. Here, we show data for the first ten wave cycles of an experiment. Several similarities with Figure 12 are apparent. First, the wavebreaking regions again occur at the base of weak density gradient regions. Second, around t = 4 min, the top of the breaking region is at a depth of approximately 15 cm and occurs at the trough of the bottom wave, consistent with the data in Figure 12. What is different in this figure with the longer time trace is that the top and bottom of the wavebreaking

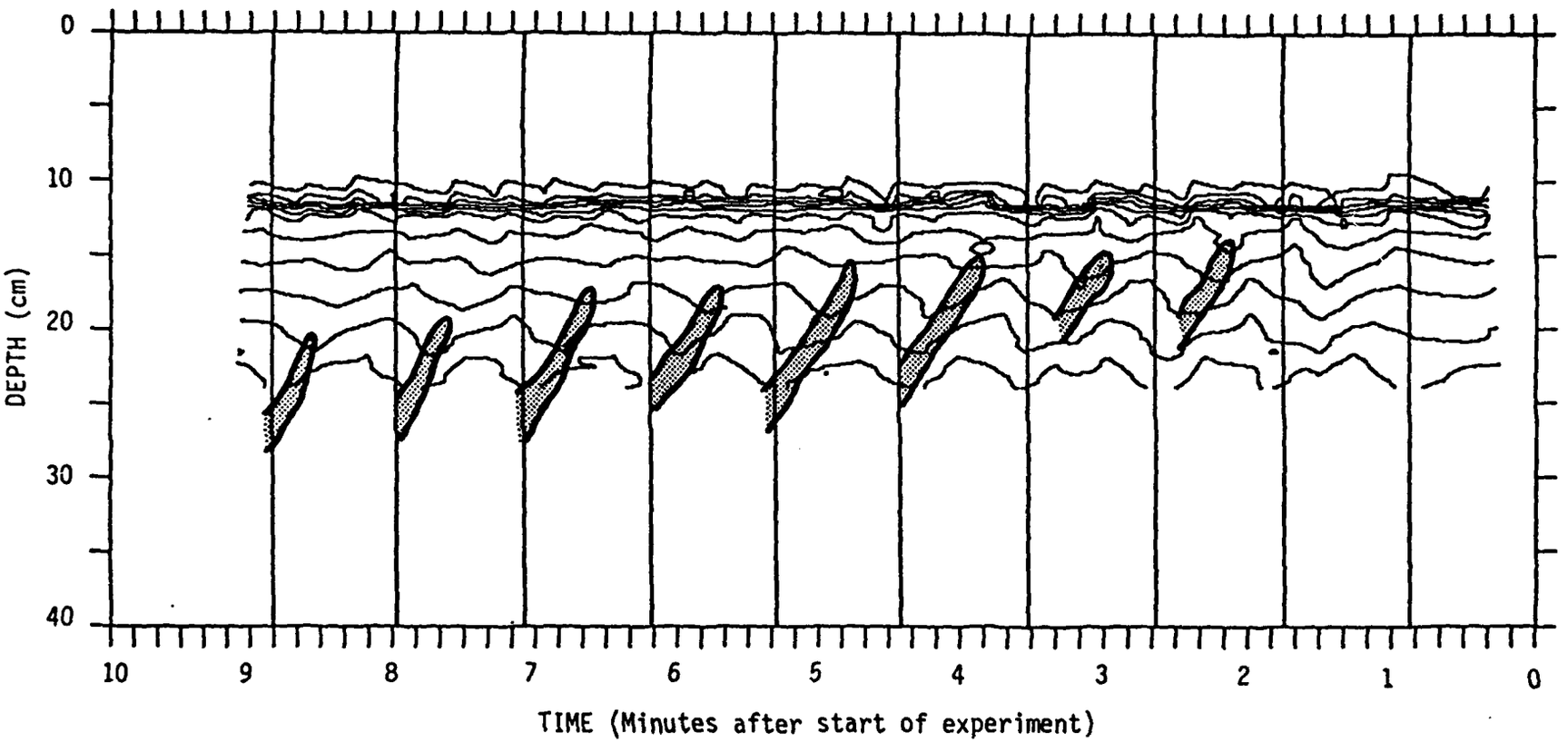

Figure 13. Contours of constant density for Case B. Shaded regions are regions of observed wavebreaking.

region occur lower in the tank with increasing time. (Note that the same tendency is shown in Figure 12, but is more difficult to see due to the smaller number of wave cycles.)

Figure 14 shows an instantaneous velocity profile obtained from one streak photograph in Case A. The solid line in this figure is a subjective fit through the data points, and the dashed line is the mean velocity profile at the start of the experiment. The critical level at the start of the experiment is at $Z/Z_{max} = 0.69$. Note that the vertical wavelength decreases as the critical level is approached, consistent with numerical gravity wave/critical level studies.

To obtain the mean velocity profile at a time during the run, we analyzed a series of streak photographs taken at periodic intervals over one cycle of the bottom forcing wave. The average of these instantaneous velocity profiles gives the mean profile.

An example of this method of obtaining the mean profile is shown in Figure 15. Here, one thin, solid line is identical to that in Figure 14, and the other three thin, solid lines are instantaneous profiles taken at other phases of the bottom wave cycle. The heavy, solid line is the average of the four instantaneous profiles. The dashed line is again the mean velocity profile at the start of the experiment. Note the modification for the mean flow in the depth range $0.35 < Z/Z_{max} < 0.7$, consistent with that predicted by numerical codes (cf., Dunkerton and Fritts, 1984).

The evolution of the mean velocity profile with time is shown in Figure 16. Note that the mean flow ledge observed in Figure 15 at t = 5 min progresses downward at t = 10, and that the rate of downward movement is approximately the same as the rate of descent of the wavebreaking in Figure 13.

At later times, the flow gradually progresses from the overturning described above to a flow characterized by one or more internal mixing regions. This flow is shown schematically

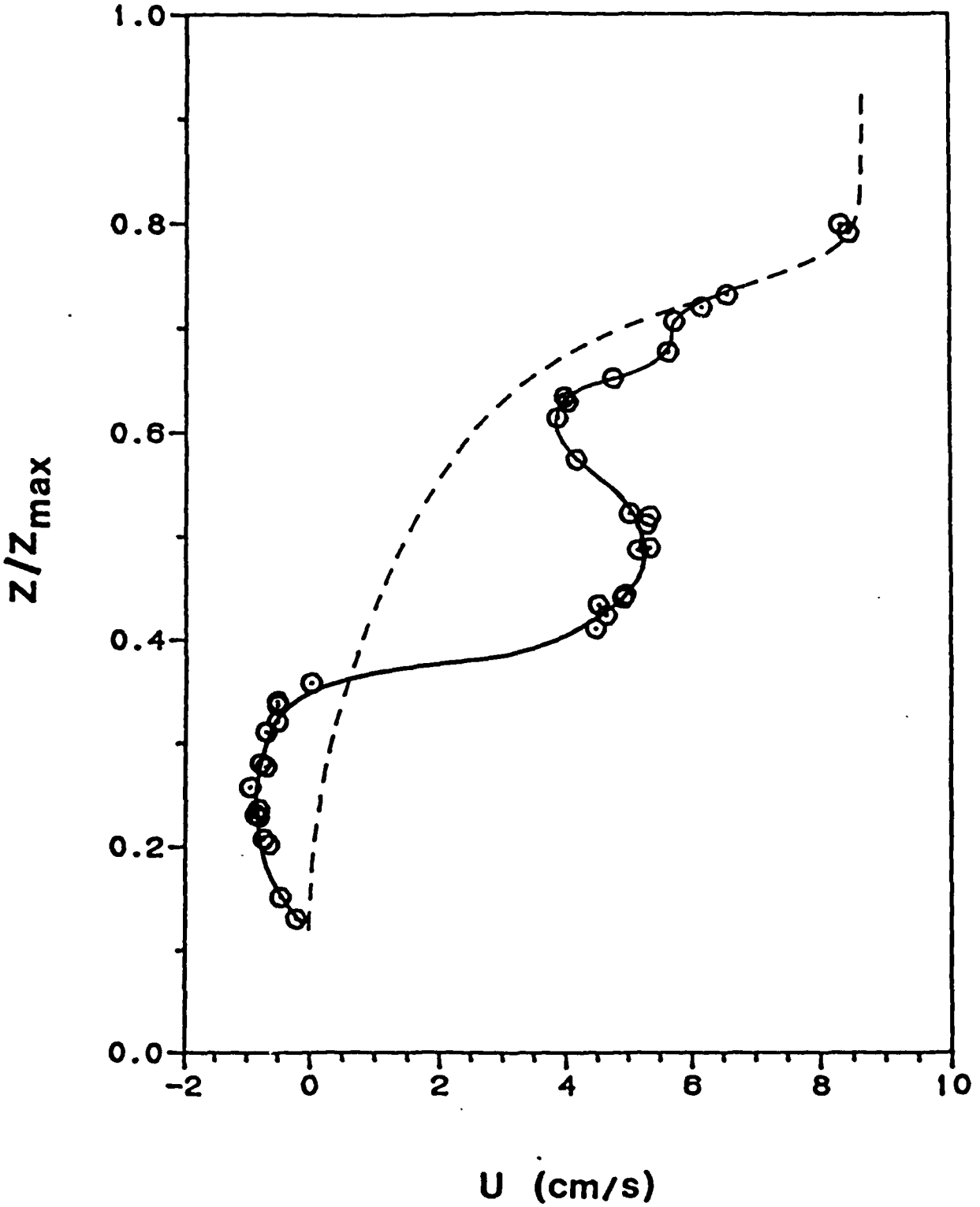

Figure 14. Instantaneous velocity profile around t = 5:00. Dashed line is the initial profile.

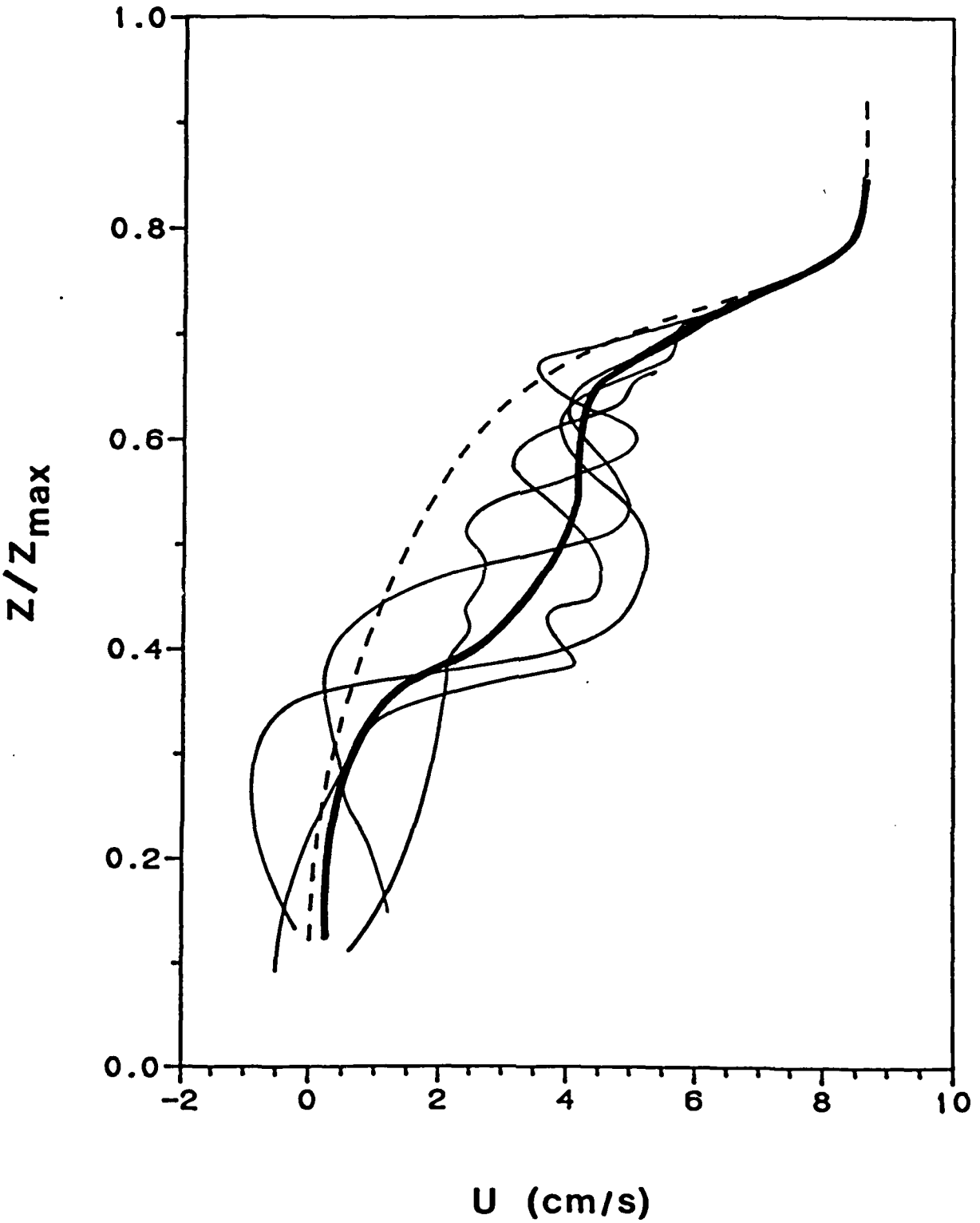

Figure 15. Thin lines are instantaneous profiles at four phases of a bottom wave cycle. Heavy line is the mean profile. Dashed line is the initial profile.

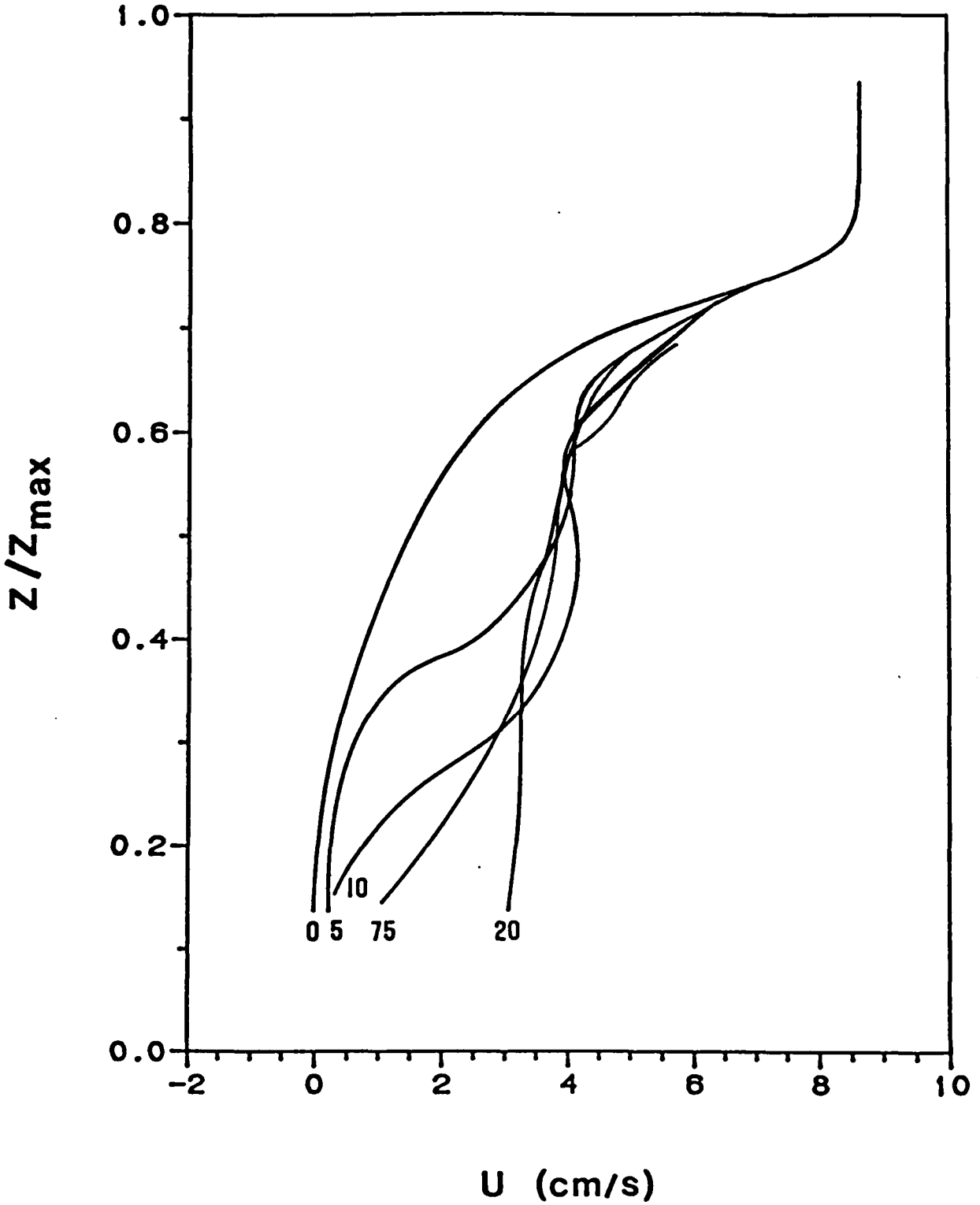

Figure 16. Evolution of the mean velocity profile with time (minutes after the start of the bottom waves).

in Figure 17 and is characterized by lens-shaped masses of fluid propagating around the tank with the bottom wave. The mixing regions have an abrupt front and consistently exhibit overturning on the bottom edge and sometimes on the upper edge. The bottom mixing region appears to coincide with a jet in the velocity profile and to ride on a sharp density striation. The regions above and below the jet appear to be conducive to K-H instabilities.

3.2. Numerical Results

The numerical code we used is that described in Fritts (1979, 1982) and Dunkerton and Fritts (1984) and will not be described here. Several numerical simulations were performed using laboratory data to initialize the code, and we will discuss three cases corresponding to Case B. In all three cases, the initial density profile, initial velocity profile, and horizontal wavelength and phase speed of the bottom wave used in the numerical code were similar to the laboratory data. Only the amplitude of the bottom forcing wave was varied in the calculations.

Figure 18 shows density contours for a linear calculation at times of t = 4, 8, and 12 min. The linear calculation does not allow for mean flow modification; hence, the mean flow velocity profile for this case does not change with time. Figure 18 shows that the predicted wavebreaking always occurs at the top of the computational domain and does not progress downward with time. Thus, neither the wavebreaking region nor the mean flow change with time in this calculation, yet both of these changes are observed in the laboratory data (Figures 13 and 16). Thus, the linear calculation is not a realistic simulation of the laboratory case.

Figure 19 shows the results of a quasi-linear calculation using the same data as in Figure 18. Here we see that, by t = 8

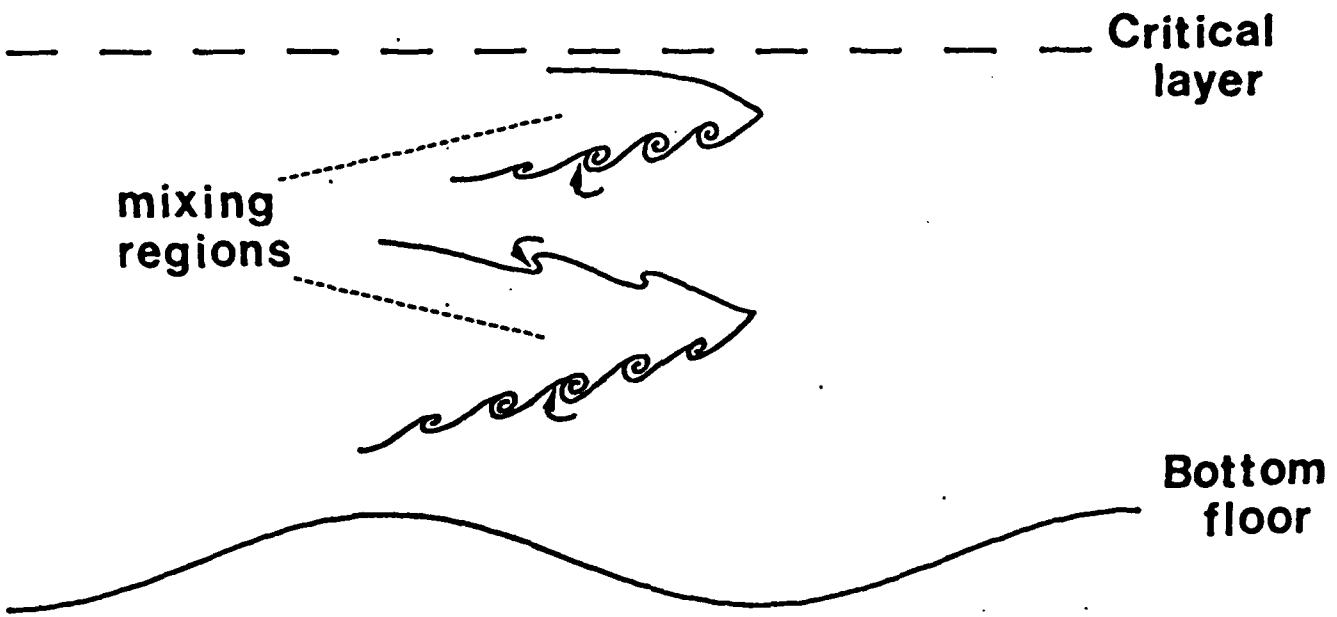

Figure 17. Schematic drawing of the late-time mixing regions. Arrows indicate the direction of the rolling motions.

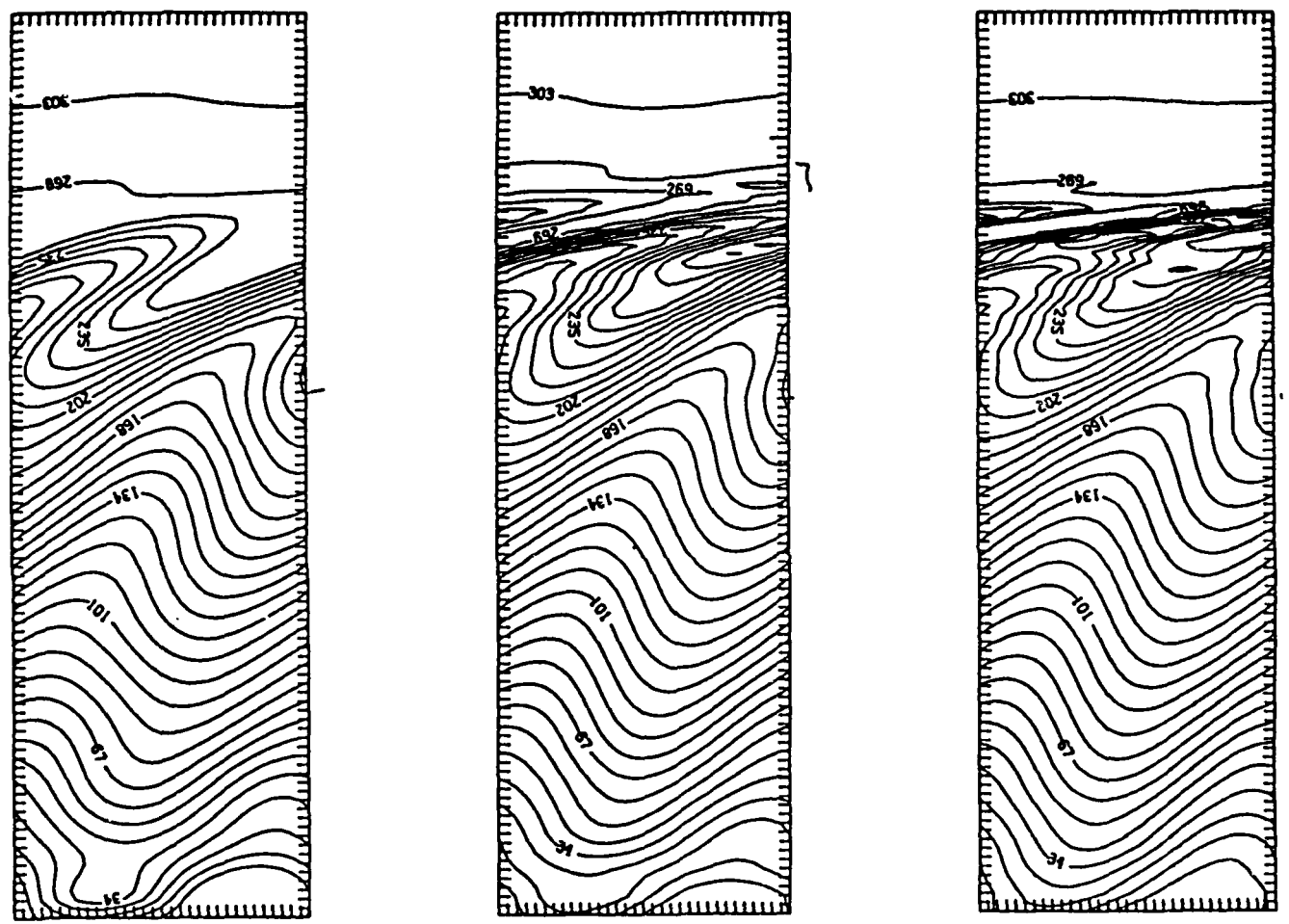

Figure 18. Contours of constant density for a linear numerical calculation at times of t = 4 (left), 8 (middle), and 12 (right) minutes.

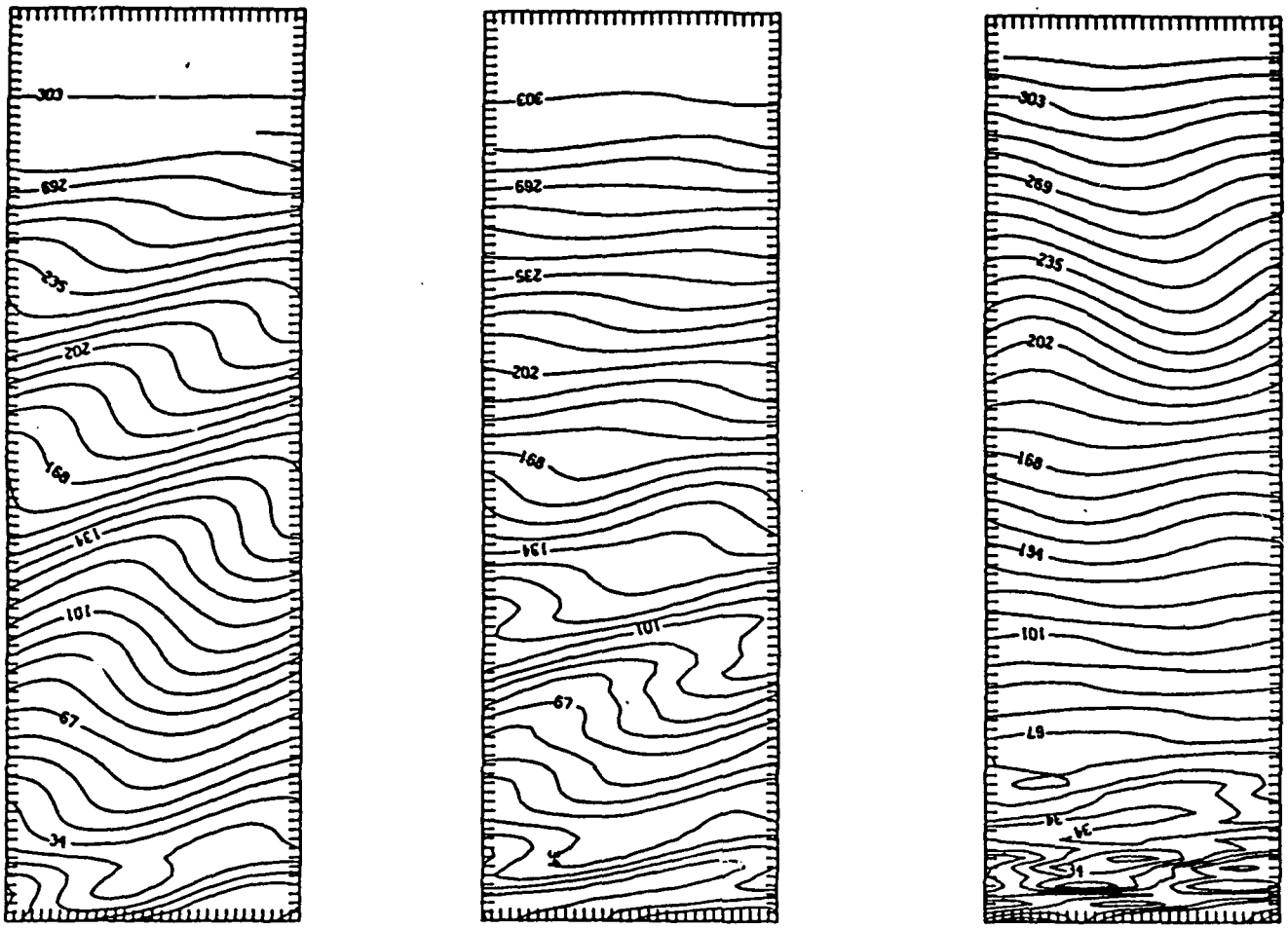

Figure 19. As in Figure 18 except quasi-linear calculation (mean flow changes with time).

min, the wavebreaking is nearly at the bottom floor. This descent is far more rapid than observed in the laboratory measurements.

It had been speculated that, because of viscous effects at the bottom floor of the tank, only a fraction of the bottom wave amplitude was being transmitted to the fluid. The rapid descent of the wavebreaking region seen in Figure 19 supports this hypothesis. To examine this effect further, several calculations were performed with a reduced amplitude.

Figure 20 shows the results of a quasi-linear calculation for an amplitude one-half that used in the laboratory experiments. Figures 20a and 20b show density contours and the evolution of the mean velocity profile, respectively, for times of t = 4, 8, 12, and 16 min. Here, the wavebreaking region descends with time, as observed in the laboratory data. The mean flow profile also shows the ledge descending with time. The ledge, however, is sharper than observed in the laboratory and does not descend as quickly as in the laboratory measurements (Figure 16).

Figure 21 shows results similar to Figure 20 but for an amplitude one-third that used in the laboratory experiments. Here, the flow is stable (no overturning was observed), and the mean flow modifications are small.

These results indicate that approximately one-half the input amplitude of the laboratory forcing wave was transmitted to the fluid. The numerical simulations agree qualitatively, but not quantitatively, with the early-time laboratory results, the laboratory mean flow ledge descending faster than the numerical predictions and the ledge being less sharp and more diffused than in the code.

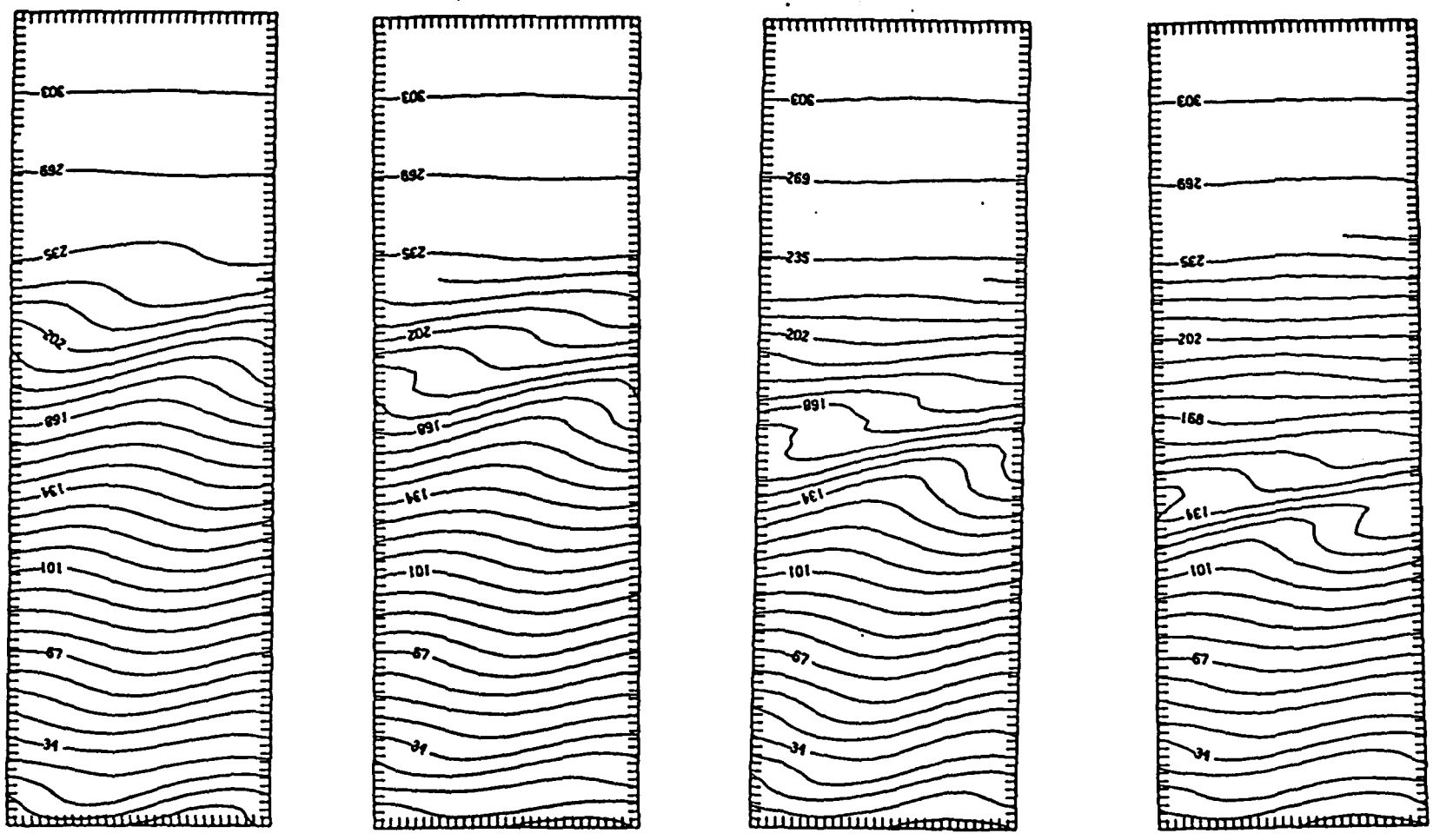

Figure 20a. Contours of constant density for a quasi-linear numerical calculation with half the forcing amplitude used in Figures 18 and 19. Times are t = 4 (left), 8, 12, and 16 (right) minutes.

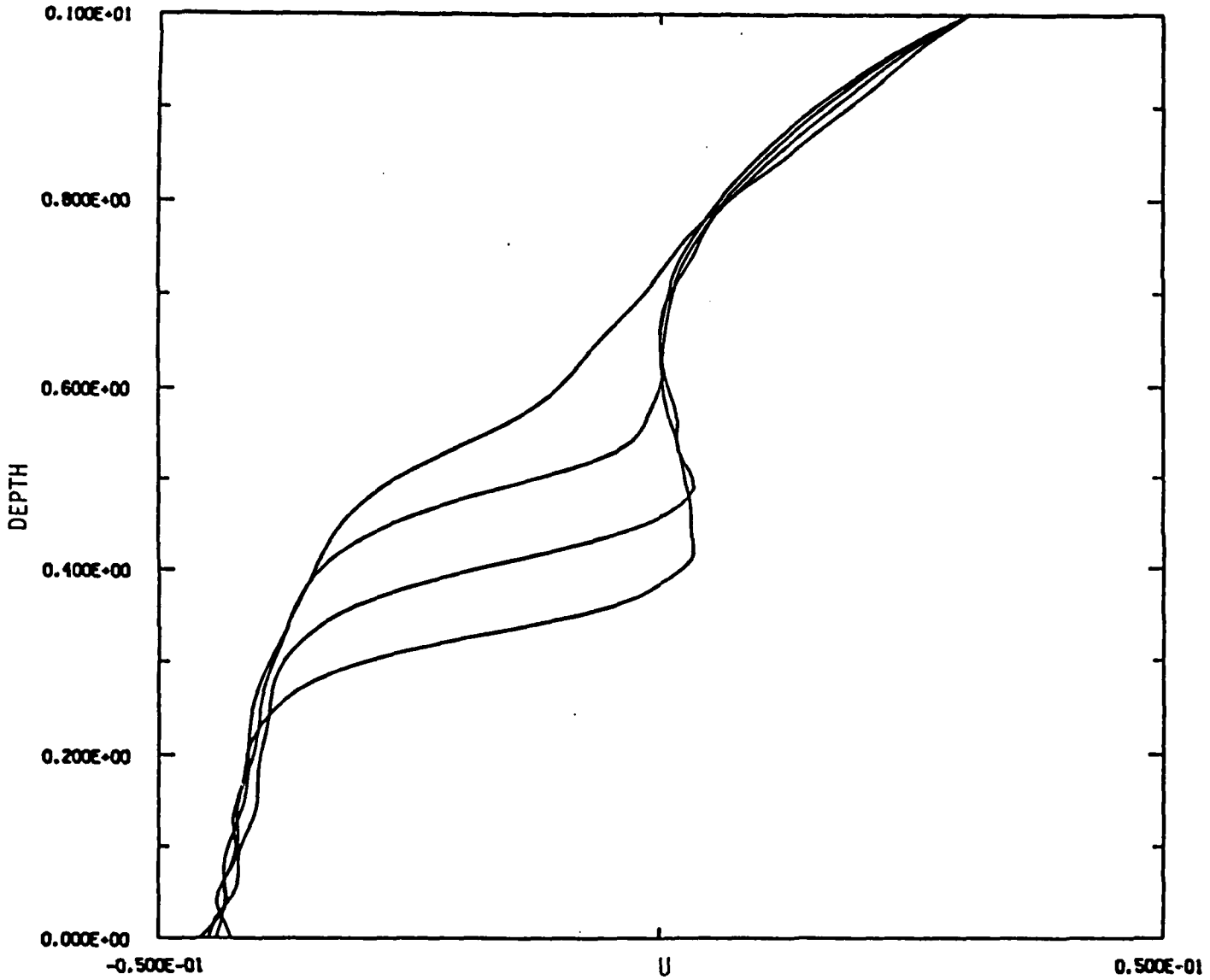

Figure 20b. Mean flow profiles for the data in Figure 20a. Times are t = 4 (top), 8, 12, and 16 (bottom) minutes.

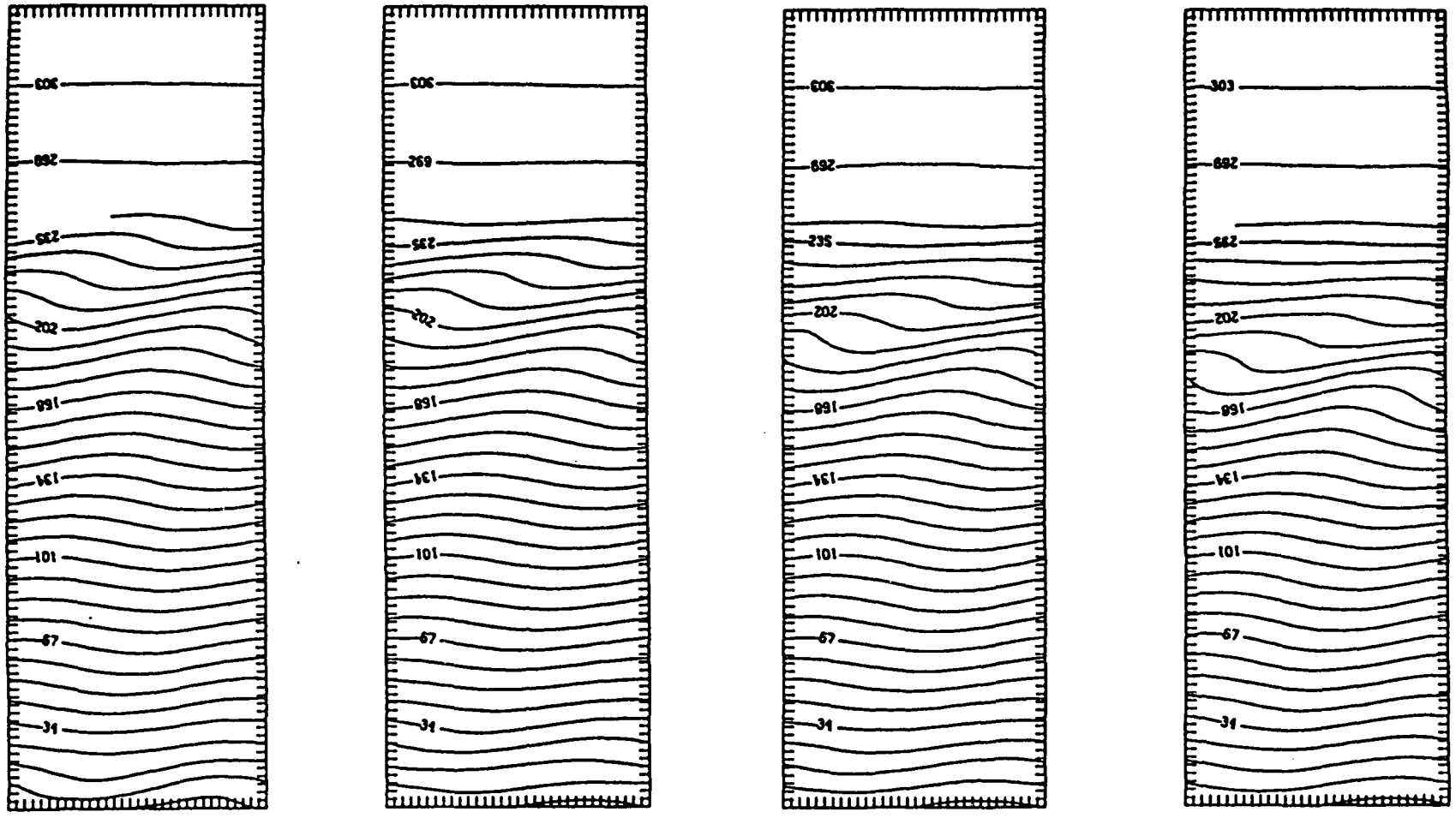

Figure 21a. As in Figure 20a with a forcing amplitude one-third that used in Figures 18 and 19.

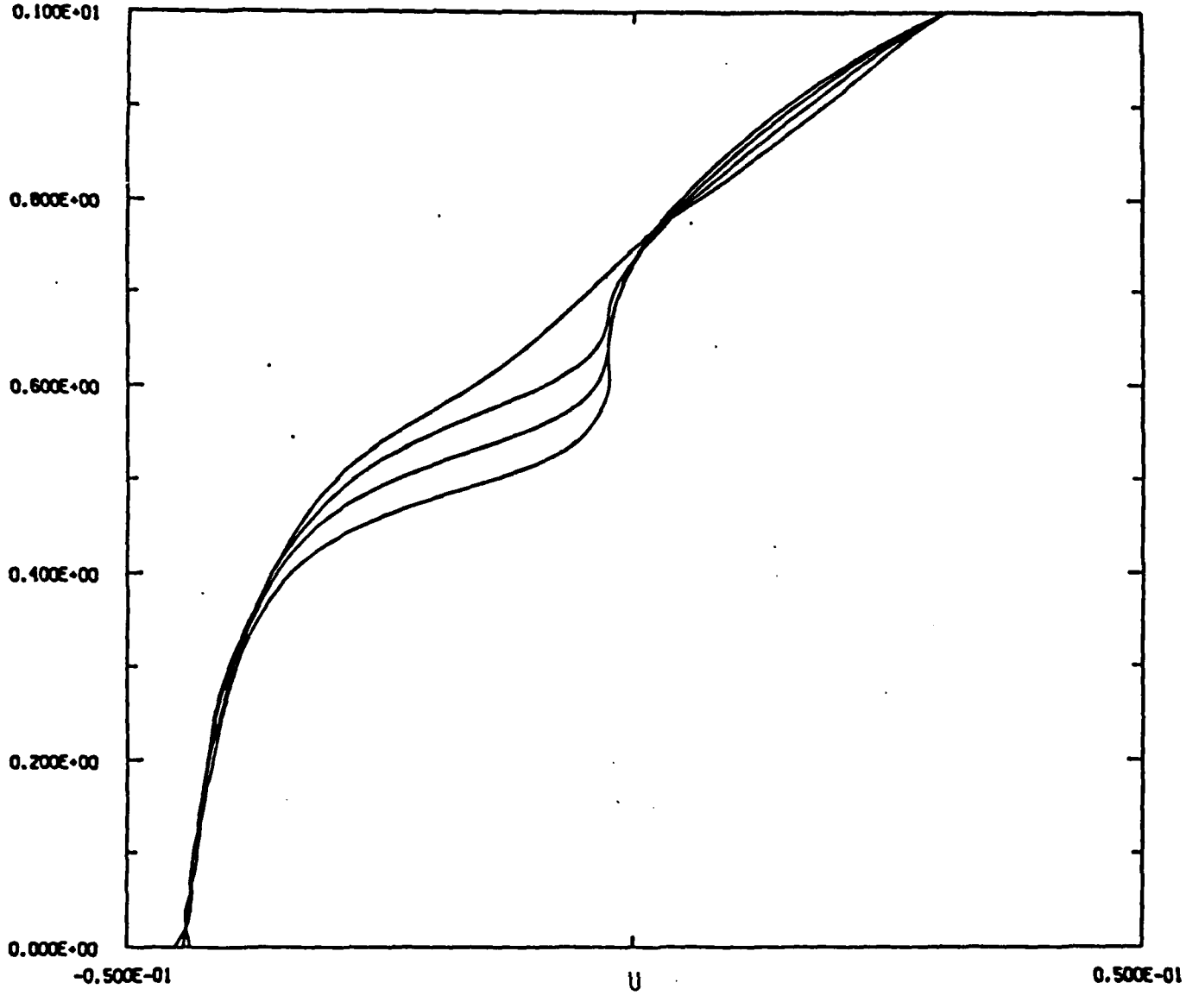

Figure 21b. Mean flow profiles for the data in Figure 21a.

4. Papers and Presentations

4.1. Papers

The following paper has been accepted for publication in Pure and Applied Geophysics (a copy is attached as Appendix A):

Delisi, D. P. and T. J. Dunkerton (1988), "Laboratory Observations of Gravity Wave Critical-Layer Flows," to appear.

The following paper appears in the Proceedings of the Eighth Symposium on Turbulence and Diffusion of the American Meteorological Society:

Delisi, D.P. and T.J. Dunkerton (1988), "Laboratory Observations of Turbulent Gravity Wave/Critical Layer Interactions."

The following paper is being prepared for submission to the Journal of the Atmospheric Sciences:

Delisi, D. P., T. J. Dunkerton, and D. C. Fritts (1988), "Laboratory and Numerical Studies of Gravity Wave/Mean Flow Interactions."

4.2. Presentations

The results from this study have been presented in the following meetings and seminars:

Delisi, D. P. and T. J. Dunkerton, "Laboratory Observations of Internal Wave/Mean Flow Interactions," Joint International Workshop on Gravity Waves and Turbulence in the Middle Atmosphere (GRATMAP), University of Adelaide, Adelaide, Australia, 20-23 May 1987.

Delisi, D. P. and T. J. Dunkerton, "Laboratory Observations of Gravity Wave Critical Layer Interactions," University of Washington Small Scale Mixing Seminar Series, Seattle, WA, 29 February 1988.

Delisi, D. P. and T. J. Dunkerton, "Laboratory Observations of Turbulent Gravity Wave/Critical Layer Interactions," Eighth Symposium On Turbulence and Diffusion of the American Meteorological Society, San Diego, CA, 26-29 April, 1988.

Delisi, D.P., "Laboratory Observations of Gravity Wave/Mean Flow Interactions," Geophysical Fluid Dynamics Laboratory/NOAA, Princeton University, Princeton, NJ, 15 July 1988.

5. Personnel

Dr. Donald P. Delisi of Northwest Research Associates, Inc. (NWRA) was the Principal Investigator for this study and was in charge of the laboratory experiments. A publication list for Dr. Delisi appears below. Dr. Timothy J. Dunkerton, also at NWRA, performed analytical studies and assisted in obtaining and interpreting the laboratory data. Dr. David C. Fritts of the University of Alaska performed the numerical simulations.

PUBLICATION LIST FOR
DONALD P. DELISI

1. Delisi, D.P. and G.M. Corcos, 1973: A study of internal waves in a wind tunnel. Boundary-Layer Meteor., 5, 121-137.

2. Stegen, G.R., D.P. Delisi, and R.C. Von Colln, 1975: A portable, digital recording, expendable bathythermograph (XBT) System. Deep-Sea Res., 22, 447-453.

3. Delisi, D.P. and G.R. Stegen, 1975: Recent experience with the DRXBT. Proc: Third STD Conf., 83-91.

4. Delisi, D.P., and I. Orlanski, 1975: On the role of density jumps in the reflexion and breaking of internal gravity waves. J. Fluid Mech., 69, 445-464.

5. Delisi, D.P. and R.H. Kirchhoff, 1977: Measurements of density and density gradient with an oscillating conductivity probe. Proc. 1977 Flow Measurement Symp., Nat. Bur. of Stand. Pub. 484, 783-802.

6. Liu, H.T., J.T. Lin, D.P. Delisi, and F.A. Robben, 1977: Application of a fluorescence technique to dye-concentration measurements in a turbulent jet. Proc. 1977 Flow Mesurement Symp., Nat. Bur. of Stand. Pub. 484, 423-446.

7. Dunkerton, T.J. and D.P. Delisi, 1984: Climatology of the equatorial lower stratosphere: An observational study. J. Atmos. Sci., 42, 376-396.

8. Dunkerton, T.J. and D.P. Delisi, 1985: The subtropical mesospheric jet observed by Nimbus 7 LIMS. J. Geophys. Res., 90, 10,681-10,692.

9. Dunkerton, T.J. and D.P. Delisi, 1986: Evolution of potential vorticity in the winter stratosphere of January-February 1979. J. Geophys. Res., 91, 1199-1208.

10. Delisi, D.P., R.E. Robins, and R.D. Lucas, 1987: The evolution of a vortex pair in stratified shear flows. Proceedings, Third International Symposium on Stratified Flows, Vol. 1, Pasadena, CA.

11. Delisi, D.P. and T.J. Dunkerton, 1988: Equatorial semiannual oscillation in zonally averaged temperature observed by the Nimbus 7 SAMS and LIMS. J. Geophys. Res., 93, 3899-3904.

12. Dunkerton, T.J., D.P. Delisi, and M.P. Baldwin, 1988: Distribution of major stratospheric warmings in relation to the quasi-biennial oscillation. Geophys. Res. Lett., 15, 136-139.

13. Delisi, D.P. and T.J. Dunkerton, 1988: Laboratory observations of turbulent gravity wave/critical layer interactions. Proceedings, Eighth Symposium on Turbulence and Diffusion of the American Meteorological Society, 70-72.

14. Delisi, D.P. and T.J. Dunkerton, 1988: Laboratory observations of gravity wave critical-layer flows. Pure and Applied Geophys., to appear.

15. Delisi, D.P. and T.J. Dunkerton, 1988: Seasonal asymmetry of the semiannual oscillation. J. Atmos. Sci., to appear.

16. Delisi, D.P., R.E. Robins, and R.D. Lucas, 1988: The evolution of a vortex pair in stratified shear flows: Laboratory results. In preparation.

17. Robins, R.E. and D.P. Delisi, 1988: The evolution of a vortex pair in stratified shear flows: Numerical results. In preparation.

ACKNOWLEDGEMENTS

Dr. Timothy J. Dunkerton participated in many valuable discussions and assisted in many of the laboratory experiments. Dr. David C. Fritts performed the numerical simulations and contributed to many lively discussions. Support in designing and building the facility and performing the experiments was provided by J. Francis Smith, Dr. Robert B. Fraser, and Lee E. Piper. The support and encouragement of, Lt. Col. Ted Cress, Lt. Col. Gerald J. Dittberner, and Lt. Col. James P. Koermer, of AFOSR, are gratefully acknowledged.

REFERENCES

Andrews, D.G., J.R. Holton, and C.B. Leovy, 1987: Middle Atmosphere Dynamics. Academic Press, New York.

Benney, D.J. and R.F. Bergeron, 1969: A New Class of Nonlinear Waves in Parallel Flows. Stud. Appl. Math., 48, 181-204.

Booker, J.R. and F.P. Bretherton, 1967: The Critical Layer for Internal Gravity Waves in a Shear Flow. J. Fluid Mech., 27, 513-539.

Bretherton, F.P., 1966: The Propagation of Internal Gravity Waves in a Shear Flow. Quart. J. Roy. Meteor. Soc., 92, 446-480.

Bretherton, F.P., P. Hazel, S.A. Thorpe, and I.R. Wood, 1967: Appendix to the paper by P. Hazel, The Effect of Viscosity and Heat Conduction on Internal Gravity Waves at a Critical Level. J. Fluid Mech., 30, 775-783, (Appendix on pp. 781-783.)

Brown, S.N. and K. Stewartson, 1980: On the Nonlinear Reflexion of a Gravity Wave at a Critical Level. Part 1. J. Fluid Mech., 100, 577-595.

Deardorff, J.W. and S.-C.Yoon, 1984: On the Use of an Annulus to Study Mixed-Layer Entrainment. J. Fluid Mech., 142, 97-120.

Delisi, D.P. and G. Corcos, 1973: A Study of Internal Waves in a Wind Tunnel. Boundary-Layer Meteorol., 5 , 121-137.

Delisi, D.P. and T.J. Dunkerton, 1988a: Equatorial Semiannual Oscillation in Zonally Averaged Temperature Observed by the Nimbus 7 LIMS and SAMS. J. Geophys. Res., 93, 3899-3904.

Delisi, D.P. and T.J. Dunkerton, 1988b: Seasonal Variation of the Semiannual Oscillation. J. Atmos. Sci., to appear.

Delisi, D.P. and R.H. Kirchhoff, 1977: Measurements of Density and Density Gradient with an Oscillating Conductivity Probe.

Proc. 1977 Flow Measurement Symp., Nat. Bur. of Stand. Pub. 484, 783-802.

Delisi, D.P. and I. Orlanski, 1975:, On the Role of Density Jumps in the Reflexion and Breaking of Internal Gravity Waves. J. Fluid Mech., 69, 445-464.

Dunkerton, T.J., 1979: On the Role of the Kelvin Wave in the Westerly Phase of the Semiannual Zonal Wind Oscillation. J. Atmos. Sci., 36, 32-41.

Dunkerton, T.J., 1980: A Lagrangian Mean Theory of Wave, Mean-flow Interaction with Applications to Nonacceleration and its Breakdown. Rev. Geophys. Space Phys., 18, 387-400.

Dunkerton, T.J. 1981: Wave Transience in a Compressible Atmosphere, Part I: Transient Internal Wave, Mean-Flow Interaction. J. Atmos. Sci., 38, 281-297.

Dunkerton, T.J., 1982a: Wave Transience in a Compressible Atmosphere, Part 3: The Saturation of Internal Gravity Waves in the Mesosphere. J. Atmos. Sci., 39, 1042-1051.

Dunkerton, T.J., 1982b: Stochastic Parameterization of Gravity Wave Stresses. J. Atmos. Sci., 39, 1711-1725.

Dunkerton, T.J., D.P. Delisi, and M.P. Baldwin, 1988: Distribution of Major Stratospheric Warmings in Relation to the Quasi-Biennial Oscillation. Geophys. Res. Lett., 15, 136-139.

Dunkerton, T.J. and D.C. Fritts, 1984: Transient Gravity Wave-Critical Layer Interaction. Part I: Convective Adjustment and the Mean Zonal Acceleration. J. Atmos. Sci., 41, 992-1007.

Fritts, D.C., 1979: The Excitation of Radiating Waves and Kelvin-Helmholtz Instabilities by the Gravity Wave-Critical Layer Interaction. J. Atmos. Sci., 36, 12-23.

Fritts, D.C., 1982: The Transient Critical-Level Interaction in A Boussinesq Fluid. J. Geophys. Res., 87, 7997-8016.

Fritts, D.C., 1984: Gravity Wave Saturation in the Middle Atmosphere: A Review of Theory and Observations. Rev. Geophys. and Space Phys., 22, 275-308.

Garcia, R.R. and S. Solomon, 1987: A Possible Relationship Between Interannual Variability in Antarctic Ozone and the Quasi-Biennial Oscillation. Geophys. Res. Lett., 14, 848-851.

Grimshaw, R., 1975: Nonlinear Internal Gravity Waves and Their Interaction with the Mean Wind. J. Atmos. Sci., 32, 1779-1793.

Holton, J.R. and R.S. Lindzen. 1972: An Updated Theory for the Quasi-Biennial Cycle of the Tropical Stratosphere. J. Atmos. Sci., 29, 1076-1080.

Kato, H. and O.M. Phillips, 1969: On the Penetration of a Turbulent Layer Into Stratified Fluid. J. Fluid Mech., 37, 643-655.

Koop, C.G., 1981: A Preliminary Investigation of the Interaction of Internal Gravity Waves with a Steady Shearing Motion. J. Fluid Mech., 113, 347-386.

Koop, C.G. and B. McGee, 1986: Measurements of Internal Gravity Waves in a Continuously Stratified Shear Flow. J. Fluid Mech., 172, 453-480.

Lindzen, R.S., 1981: Turbulence and Stress Due to Gravity Wave and Tidal Breakdown. J. Geophys. Res., 86C, 9707-9714.

Maslowe, S.A., 1973: Finite-Amplitude Kelvin-Helmholtz Billows. Bound-Layer Meteor., 5, 43-52.

Maslowe, S.A., 1977: Weakly Nonlinear Stability Theory of Stratified Shear Flows. Quart. J. Roy. Meteor. Soc., 103, 769-783.

Maslowe, S.A., 1986: Critical Layers in Shear Flows. Ann. Rev. Fluid Mech., 18, 405-432.

Orlanski, I. and K. Bryan, 1969: Formation of the Thermocline Step Structure by Large-Amplitude Internal Gravity Waves. J. Geophys. Res., 74, 6975-6983.

Plumb, R.A. and A.D. McEwan, 1978: The Instability of a Forced Standing Wave in a Viscous Stratified Fluid: A Laboratory Analogue of the Quasi-Biennial Oscillation. J. Atmos. Sci., 35, 1827-1839.

Scranton, D.R. and W.R. Lindberg, 1983. An Experimental Study of Entraining, Stress-Driven, Stratified Flow in an Annulus. Phys. Fluids, 26, 1198-1205.

Thorpe, S.A., 1973: Turbulence in Stably Stratified Fluids: A Review of Laboratory Experiments. Boundary-Layer Meteor., 5, 95-119.

Thorpe, S.A., 1981: An Experimental Study of Critical Layers. J. Fluid Mech., 103, 321-344.

Appendix A

LABORATORY OBSERVATIONS OF GRAVITY WAVE CRITICAL-LAYER FLOWS

By

Donald P. Delisi

and

Timothy J. Dunkerton

Northwest Research Associates, Inc.
P.O. Box 3027
Bellevue, WA 98009
USA

September, 1987

Revised April, 1988

Pure and Applied Geophysics, to appear.

ABSTRACT

A new laboratory facility for studying gravity wave critical-layer interactions is described, and the results from one experiment are presented. In the experiment, a forced, monochromatic gravity wave is allowed to propagate into a stratified shear flow containing a critical level for the gravity wave. The early evolution of the flow is characterized by turbulent wavebreaking and mean flow modifications which are in qualitative agreement with previous numerical simulations. The late-time critical layer flow is characterized by internal mixing regions which are phase-locked to the incoming gravity wave.

1. Introduction

Atmospheric gravity waves exist over a broad range of frequencies and wavelengths. These waves have two features which make them important for the earth's general circulation: their ability to transport momentum vertically and their potential to generate turbulence and, thereby, produce mixing. A shear flow can have significant effects on gravity wave propagation. As a wave approaches its critical level (where the phase speed of the wave equals the mean flow speed; Booker and Bretherton, 1967), the wave's vertical propagation is severely modified, wave energy is transferred to the mean flow, and turbulence can be generated by unstable breakdown.

Most of our present understanding of these gravity wave critical-level interactions comes from theoretical and numerical research (e.g., Bretherton, 1966; Benney and Bergeron, 1969; Maslowe, 1973, 1977; Grimshaw, 1975; Fritts, 1978, 1979, 1982; Brown and Stewartson, 1980; Dunkerton, 1980, 1981, 1982; Lindzen, 1981; Dunkerton and Fritts, 1984; and many others - for recent reviews, see Fritts, 1984 and Maslowe, 1986). Observationalists have attempted to isolate and study these interactions (Merrill and Grant, 1979) as well as equatorial wave, mean-flow interactions (Wallace and Kousky, 1968). However, it has been difficult to locate critical levels accurately and to observe the interactions quantitatively. Similar difficulties have occurred in the ocean.

Because of our inability to study these interactions in the atmosphere, it is useful to observe them under controlled laboratory conditions. Five previous experimental studies of gravity wave-critical level interactions have been reported. The earliest three studies (Bretherton *et al*, 1967; Thorpe, 1973; and Koop, 1981) were qualitative in nature and were somewhat cursory in that they were reported either in an appendix to a main paper or as part of a much larger investigation. In a more extensive, but still qualitative, study, Thorpe (1981) performed a flow-visualization study of these interactions. In the most recent study, Koop and McGee (1986) followed up on Koop's earlier work (1981) and compared their flow visualization and probe measurements to results from a numerical model.

As pioneering as these earlier studies are, they are by no means complete. This is due to the difficulty in establishing a controlled stratified shear flow in the laboratory and propagating known internal waves into that flow. Thus, nearly all of the previous results are qualitative in nature, with few quantitative measurements. Previous studies have also been limited in the evolution times which could be investigated. These temporal constraints are the result of the experimental facilities used to study the flows. The tilting tanks used by Bretherton *et al* (1967) and Thorpe (1973, 1981) have a limited running time before surges from the end walls destroy the flow. Similarly, the temporal evolution in the recirculating tank used by Koop (1981) and Koop and McGee (1986) is limited by the physical dimensions of the test section and the dimensions and towing speeds of the

internal wave sources. A second limitation on long-time evolution in their facility is the non-steadiness of their velocity and density profile over time scales of approximately ten minutes (Koop, 1981, figures 4 and 6). This non-steadiness is due to the small but noticeable effect of mixing caused by the pump which is generating their shear flow.

Here, we describe a new laboratory facility for studying gravity wave critical-level interactions, and we present results from one experiment. The facility is a modification of that developed by Plumb and McEwan (1978) who forced a standing internal gravity wave in a cylindrical annulus of stratified salt water and generated an analogue of the equatorial stratospheric quasi-biennial oscillation. In this study, we force propagating internal gravity waves into a stratified salt water flow with shear and observe the resulting interactions. Our ultimate goal is to obtain quantitative measurements of both the early evolution and the long-time evolution of critical layer interactions under a variety of experimental conditions.

2. The Experimental Facility

The experiment was performed in an annular tank having an outer diameter of 1.8 m, an inner diameter of 1.2 m, and a depth of 40 cm (Figure 1). The sides of the tank are made of clear acrylic to allow us to observe the flow inside the tank.

The bottom of the tank is comprised of an 0.6 cm thick rubber sheet overlaying thirty-two 1.0 cm thick acrylic sheets of equal size and shape. Each acrylic sheet covers nearly the full width of the annulus and touches adjacent sheets on two sides, forming a continuous ring around the bottom of the tank. The common boundary of each pair of acrylic sheets rests on top of a vertical piston. These pistons are each driven by a stepper motor which is under computer control. In an experiment, the computer instructs the pistons to drive the bottom floor of the tank up and down, generating a wave of prescribed amplitude and phase speed which progresses around the tank. The acrylic sheets provide structural rigidity between pistons, and the rubber sheet acts both as a water seal at the bottom of the tank and as a stretching membrane between the acrylic sheets and the sides of the tank.

The wave tank is filled using two 300-liter storage tanks. The filling method is similar to that of Fortuin (1960), Delisi and Orlanski (1975), and others, and yields density profiles which are nearly exactly linear. In our experiment, we use four linear density regions in the density profile (the dashed line in Figure 2 shows the measured density profile before the lid is

started; in Figure 2 and following figures, the height above the bottom floor is normalized by the total water depth, Z_{max} = 38.7 cm). The top region is 10 cm thick, with a Brunt-Vaisala frequency, N = 1.63 sec^{-1}, defined by

$$N = \left[- \frac{g}{\bar{\rho}} \frac{\partial \rho}{\partial z} \right]^{1/2}$$

where g is the acceleration due to gravity, ρ is density, $\bar{\rho}$ is average density, and z is the vertical coordinate. Below the top region are two layers each 5 cm thick where N = 1.50 and 1.25 sec^{-1}, respectively. In the lower half of the tank, N = 0.83 sec^{-1}.

We use several layers of constant density-gradient fluid because of the way we generate the shear flow and the internal waves. The shear flow is generated by rotating a lid on the water surface. The lid consists of an annular acrylic channel which floats on the water and nearly completely covers the water surface. The channel is driven by a large O-ring which runs in a groove on the outer wall of the channel and passes over four pulleys. The lid is rotated by a variable-speed motor which is connected to one of the pulleys. The lid is self-centering, adjustable in speed, and generates a solid-body velocity profile in the fluid.

Our rotating lid is a modification of a method used previously by Kato and Phillips (1969), Scranton and Lindberg (1983), Deardorff and Yoon (1984), and others to study the downward propagation of a mixed region in a density-stratified flow. In their studies, the lid consisted of a screen which was driven from the center of the tank with a rotating shaft and radial arms. They found that the depth of the mixed layer depended on the stratification of the layer into which the mixed region was growing. In order to minimize the depth of the mixed layer in our experiments, we placed a high-N region at the top of the tank next to the rotating lid.

To perform an experiment, we first fill the tank with a stratified salt solution. The lid is then started and brought up to a pre-selected speed, and the flow is allowed to reach a near-steady state. After the flow is established, the bottom floor of the tank is moved to generate internal gravity waves. Wave energy propagates vertically into the tank, and, if the phase speed of the waves is below the maximum current speed, the wave encounters a critical level. In this study, only monochromatic waves are generated. Once the floor is started, waves are generated continuously throughout the experiment.

The dissipation scale height, d, is given by

$$d \approx \frac{k \hat{c}^4}{\nu N^3}$$

where k is zonal wavenumber, $\hat{c} = c-\bar{U}$, c is the phase speed of the forced wave at the bottom floor, $\bar{U}$ is the mean flow speed, and ν is kinematic viscosity (Plumb and McEwan, 1978). The larger the dissipation scale height, the more wave energy that reaches a given vertical level above the tank floor. To maximize this wave energy and to minimize wave dissipation, we want d to be as large as possible. Thus, for a given zonal wavenumber and phase speed, we want N to be as low as possible in the bottom of the tank. (A lower constraint on N is that we have enough signal in the second derivative of density to visualize the flow using a shadowgraph.) For this reason, we have a lower value of N at the bottom of the tank than at the top of the tank (Figure 2). The two middle layers of constant N fluid act as smooth transitions between the top and bottom layers. The variations in N do not cause any noticeable wave reflection during an experiment.

Neutrally buoyant particles are added to the storage tanks before the filling process is started. Once in the tank, these particles are illuminated from the top using a 1000-watt theatrical spotlight. A 2.5-cm wide slit at the top of the viewing section allows just the particles in a given constant-radius plane to be illuminated. In this study, the illuminated plane is located 20 cm from the inner wall of the tank (5 cm from the centerline towards the outer wall of the tank). A 35-mm camera is used to obtain streaks of the moving particles. To obtain particle streaks, the film is exposed for either 1 or 4 seconds. The streaks in the resulting photographic prints are digitized

and corrected for parallax to yield instantaneous velocity profiles.

A shadowgraph is also used to visualize the flow field. A video camera and a 35-mm camera are used to record the flow field as visualized by the shadowgraph.

3. Results and Discussion

The velocity profile after the meanflow is established but before the bottom floor is started is shown in Figure 3. Results from two streak photographs are shown in this figure; the circles are from a 4-second exposure photograph, and the squares are from a 1-second exposure photograph. The 4-second photograph enables us to measure the slower moving particles with better accuracy than is possible using 1-second exposure photographs. As is evident from the figure, the 4-second and 1-second data are consistent in the range where they overlap.

The solid line in Figure 3 is a subjective fit through the data. The mixed layer is in the high-N region at the top of the tank; the velocities in this region are nearly constant. Below the mixed layer is a near-exponential profile in the horizontal speed (dashed line in Figure 3).

At a time t = 0, the bottom floor is started. The wave parameters used are the following: wavenumber = 2, amplitude = 4.0 cm (peak-to-peak), and phase speed = 4.5 cm/sec. (Due to bottom boundary layer effects, the effective amplitude transmitted to the fluid is approximately half the imposed amplitude.) From Figure 3, a phase speed of 4.5 cm/sec places the critical level at $Z/Z_{max} = 0.69$.

During the first two wave cycles, the shadowgraph shows no evidence of breaking. What is observed, however, is a dark band, tilted from the horizontal, which is located below the critical

level, and progresses down towards the bottom of the tank as the wave propagates.

During the third wave cycle, and for all wave cycles thereafter, overturning and turbulence are observed on the shadowgraph below the critical level. A schematic drawing of the early wavebreaking is shown in Figure 4. This figure shows the tank at one instant of time, as if the annulus were cut radially and spread out horizontally. The height of the bottom floor represents the forced wave which is propagating from left to right. The critical level is shown as the dashed horizontal line. Regions of wavebreaking are shown as the regions of rolling motions which are inclined from the lower left to the upper right. All observed regions of wavebreaking occur below the critical level. The dotted rectangular box represents the approximate horizontal and vertical extent of the region illuminated by the shadowgraph. Because each forced wave has a horizontal extent of half the circumference of the tank (wavenumber two), only a small portion of the wave can be visualized at any one time.

Photographs of this early wavebreaking, as visualized by the shadowgraph, are shown in Figure 5. Five examples are shown in this figure to give the reader a feeling for the kind of breaking which is observed. Initially, the observed wavebreaking occurs from just below the critical level to just below the mid-depth of the tank. In subsequent wave cycles, the breaking occurs lower in the tank, as the mean flow is modified (see below). From the videos, this early wavebreaking consists of a series of rolling

motions, alternately increasing then dying out. The rolling appears quasi-two-dimensional initially, but rapidly becomes turbulent and three-dimensional. The scales of the rolling motions increase as the breaking progresses further from the critical level, the horizontal and vertical scales being 6-10 cm and 2-3 cm, respectively, near the ciritical level, and 8-12 cm and 3-5 cm just below the mid-depth of the tank.

Figure 6 shows a streak photograph taken during the fifth wave cycle. The streaks are mostly horizontal, the particles progressing from left to right in the photograph. Just above the clock, however, the particle streaks are no longer horizontal, and rolling motions are observed. Comparisons were made between this streak photograph, a shadowgraph photograph, and the video pictures, all of which were taken at a similar phase in the bottom wave cycle. The comparisons of vertical depth and horizontal scales confirm that the rolling motions observed in Figure 6 correspond to the rolling motions and turbulence observed in the shadowgraph, similar to the photographs shown in Figure 5.

The comparisons between Figure 6 and the corresponding shadowgraph videos and photographs are confirmation that the breaking observed in the shadowgraph occurs near the center of the tank and is not a wall effect. Thus, the rolling motions and resulting turbulence are a result of the internal wave critical-level interaction and are not simply an artifact of the experimental facility.

The form of the observed, early wavebreaking is still of some conjecture. In an earlier internal wave critical-level study by Thorpe (1981), gravitational overturning was also observed, but the form of the breakdown is not discussed. In the gravity wave critical-level experiment by Koop and McGee (1986), where wavebreaking was also observed, the overturning is described as the result of convective instability. In our experiments, however, the overturning is a series of rolling motions, distinctly reminiscent of Kelvin-Helmholtz instabilities and similar to the observations of Kelvin-Helmholtz billows reported on by Thorpe (1968, 1971, 1973), Delisi and Corcos (1973), and others. From the instantaneous velocity profiles obtained from streak photographs, we have determined that the wavebreaking coincides with the region of maximum vertical shear. This observation supports the hypothesis that early wavebreaking is the result of Kelvin-Helmholtz and not convective instability. In-situ measurements are currently being planned which we hope will shed additional light on the form of the observed wavebreaking.

Around t $\sim$ 6-15 min, the flow gradually progresses from the gravity wave critical-layer structure described above to a flow characterized by one or more internal mixing regions. These regions are characterized by lens-shaped masses of fluid propagating around the tank with the bottom wave. The mixing regions have an abrupt front and consistently exhibit overturning on the bottom edge and sometimes on the upper edge. Usually, turbulence appears to exist throughout the entire mass of fluid.

Between t $\sim$ 15 - 65 min, the mixing regions are mostly distinct from the earlier critical level breaking and are not necessarily locked in phase with the forced wave. Around t = 65 min, the flow has evolved into a single mixing region which is located just below mid-depth in the tank. Often, a second, weaker mixing region is also observed above the dominant one. It may be that this weaker region is always present but is hard to discern on the shadowgraph. The mixing regions are phase-locked to the trough of the forced wave. The bottom mixing region appears to coincide with a jet in the velocity profile and to ride on a sharp density striation. This flow is shown schematically in Figure 7. This flow continues with little change to the end of the experiment, at t = 125 min.

Streak photographs have been analyzed to yield information on the instantaneous and mean velocity profiles. An example is shown in Figure 8. Here, circles indicate the measured speed of particles as a function of height above the bottom floor. The solid line is a subjective fit through the data points and represents the instantaneous velocity profile. The dashed line is the mean velocity profile at the start of the experiment (Figure 3). Note in Figure 8 that the vertical wavelength decreases as the critical level is approached (cf. mean flow in Figure 9), consistent with numerical gravity wave critical-level studies (e.g., Dunkerton and Fritts, 1984).

To obtain the mean velocity profile during the run, we analyze four streak photographs taken every quarter of a wave

period during one wave cycle. The average of these four instantaneous velocity profiles is the mean profile. An example is given in Figure 9. Here we show the data from the four streak photographs taken around t = 5 minutes (approximately the fifth wave cycle). The heavy solid line is the average of the four instantaneous profiles, while, again, the dashed line is the mean velocity profile taken at the start of the experiment (Figure 3). This figure shows that the mean velocity at t = 5 min differs from the initial profile mostly in the range $0.35 < Z/Z_{max} < 0.7$. This mean flow modification is similar to that predicted by numerical codes (Fritts, 1982; Dunkerton and Fritts, 1984; Fritts and Dunkerton, 1984).

The evolution of the mean flow with time is shown in Figure 10. Here we see that the mean flow ledge observed in Figure 9 at t = 5 min progresses downwards at t = 10 and 20 min. The mean flow at t = 75 min is similar to the mean flow at t = 20 min except near the bottom floor, where the mean flow has decelerated.

Figure 11 shows instantaneous particle velocities from four wave cycles at times of 5, 10, 20, and 75 min. The dashed line in each figure indicates the phase speed of the forced wave (4.5 cm/sec). Whenever $u' > c - \bar{U}$, the wave is convectively unstable according to Orlanski and Bryan (1969). In Figure 11, this occurs whenever an instantaneous particle velocity exceeds the wave phase speed of 4.5 cm/sec. The arrows in Figure 11 indicate the depths over which wavebreaking is observed to occur from the

video and photographs of the shadowgraph. In all cases, the observed wavebreaking is seen to extend below the region where the Orlanski-Bryan criterion is satisfied (cf, Dunkerton and Fritts, 1984). In our experiment, once initiated, wavebreaking can occur over a depth up to one-half the vertical wavelength. Thus, in Figure 11, wavebreaking can occur up to one-half a vertical wavelength below that predicted by Orlanski and Bryan. In all cases in Figure 11, the observed wavebreaking is less than one-half a vertical wavelength below that where $\bar{U} + u' = c$.

Recent experimental runs (not shown) indicate that satisfaction of the Orlanski-Bryan criterion is not necessary to produce wavebreaking. In those runs, $\bar{U} + u'$ was always less than c, yet wavebreaking occurred which was qualitatively similar to that observed here.

Finally, a density profile was made after the experiment was concluded and the fluid had come to rest. This profile is shown as the solid line in Figure 2. Two mixed layers are shown in this profile. The first layer is at the top of the tank and is due to turbulence generated by the rotating lid. The second layer is centered at $Z/Z_{max} \sim 0.43$ and is the result of fluid mixed by wavebreaking. The dominant mixing region observed in the last half of the experiment was centered at $Z/Z_{max} \sim 0.43$, but it is not known at this time whether the mixed layer at that depth is the result of the mixing region or whether the layer existed before the appearance of the mixing region.

4. Summary and Conclusions

In Section 3, we have shown laboratory results of a turbulent gravity wave critical-layer experiment. We have shown the early evolution of the critical layer interaction, which results in wavebreaking qualitatively similar to that predicted by numerical studies, as well as the long-time evolution of the critical layer, which results, at least in our experiments, in steady-state mixing regions.

The early evolution includes turbulent wavebreaking which is reminiscent of Kelvin-Helmholtz billows. Although no quantitative comparisons have been performed yet with numerical predictions, the experimental results agree qualitatively with numerical simulations in the location of the wavebreaking and in the evolution of the mean flow.

Our observations of the long-time evolution of the gravity wave critical-layer interaction were unexpected and are not well understood. The appearance of steady-state mixing regions is not unique to the experiment presented here and has been observed in several other of our laboratory critical-layer experiments. The evolution of this phenomenon clearly warrants additional investigation.

The results of this study have pointed out several areas that deserve further investigation. First, additional sensors must be utilized to obtain quantitative measurements to examine such questions as the form of the initial wavebreaking, self

acceleration of the incoming wave, reflection from the critical layer, transmission through the critical layer, and the long-time evolution of the critical layer. Second, additional experiments must be performed to examine other parameter ranges. For example, both laminar and turbulent critical layers need to be investigated. Finally, numerical predictions must be performed which simulate the laboratory environment, and quantitative comparisons must be made between the numerical simulations and the laboratory measurements. Additional experiments are currently in progress, and the results of those investigations will be presented at a later date.

ACKNOWLEDGEMENTS

The authors would like to thank David C. Fritts for many stimulating discussions during this study. We also thank J. Francis Smith, Robert B. Fraser, and Lee E. Piper for their support in designing and building the facility and assistance in performing the experiments. This study was supported by the Air Force Office of Scientific Research under contract F49620-86-C-0015.

REFERENCES

Benney, D.J. and R.F. Bergeron (1969), "A New Class of Nonlinear Waves in Parallel Flows, "Stud. Appl. Math., 48, 181-204.

Booker, J.R. and F.P. Bretherton (1967), "The Critical Layer for Internal Gravity Waves in a Shear Flow," J. Fluid Mech., 27, 513-539.

Bretherton, F.P. (1966), "The Propagation of Internal Gravity Waves in a Shear Flow," Quart. J. Roy. Meteor. Soc., 92, 446-480.

Bretherton, F.P., P. Hazel, S.A. Thorpe, and I.R. Wood (1967), Appendix to the paper by P. Hazel, "The Effect of Viscosity and Heat Conduction on Internal Gravity Waves at a Critical Level," J. Fluid Mech., 30, 775-783, (Appendix on pp. 781-783.)

Brown, S.N. and K. Stewartson (1980), "On the Nonlinear Reflexion of a Gravity Wave at a Critical Level. Part 1," J. Fluid Mech., 100, 577-595.

Deardorff, J.W. and S.-C.Yoon (1984), "On the Use of an Annulus to Study Mixed-Layer Entrainment," J. Fluid Mech., 142, 97-120.

Delisi, D.P. and G. Corcos (1973), "A Study of Internal Waves in a Wind Tunnel," Boundary-Layer Meteorol., 5, 121-137.

Delisi, D.P. and I. Orlanski (1975), "On the Role of Density Jumps in the Reflexion and Breaking of Internal Gravity Waves," J. Fluid Mech., 69, 445-464.

Dunkerton, T.J. (1980), "A Lagrangian Mean Theory of Wave, Mean-flow Interaction with Applications to Nonacceleration and its Breakdown," Rev. Geophys. Space Phys., 18, 387-400.

Dunkerton, T.J. (1981), "Wave Transience in a Compressible Atmosphere, Part I: Transient Internal Wave, Mean-Flow Interaction," J. Atmos. Sci., 38, 281-297.

Dunkerton, T.J. (1982), "Wave Transience in a Compressible Atmosphere, Part 3: The Saturation of Internal Gravity Waves in the Mesosphere," J. Atmos. Sci., 39, 1042-1051.

Dunkerton, T.J. and D.C. Fritts (1984), "Transient Gravity Wave-Critical Layer Interaction. Part I: Convective Adjustment and the Mean Zonal Acceleration," J. Atmos. Sci., 41, 992-1007.

Fortuin, J.M.H. (1960), "Theory and Application of Two Supplementary Methods of Constructing Density Gradient Columns," J. Polymer Sci., 44, 505-515.

Fritts, D.C. (1978), "The Nonlinear Gravity Wave-Critical Level Interaction," J. Atmos. Sci., 35, 397-413.

Fritts, D.C. (1979), "The Excitation of Radiating Waves and Kelvin-Helmholtz Instabilities by the Gravity Wave-Critical Layer Interaction," J. Atmos. Sci., 36, 12-23.

Fritts, D.C. (1982), "The Transient Critical-Level Interaction in A Boussinesq Fluid," J. Geophys. Res., 87, 7997-8016.

Fritts, D.C. (1984), "Gravity Wave Saturation in the Middle Atmosphere: A Review of Theory and Observations," Rev. Geophys. and Space Phys., 22, 275-308.

Fritts, D.C. and T.J. Dunkerton (1984), "A Quasi-Linear Study of Gravity-Wave Saturation and Self-Acceleration," J. Atmos. Sci., 41, 3272-3289.

Grimshaw, R. (1975), "Nonlinear Internal Gravity Waves and Their Interaction with the Mean Wind," J. Atmos. Sci., 32, 1779-1793.

Kato, H. and O.M. Phillips (1969), "On the Penetration of a Turbulent Layer Into Stratified Fluid," J. Fluid Mech., 37, 643-655.

Koop, C.G. (1981), "A Preliminary Investigation of the Interaction of Internal Gravity Waves with a Steady Shearing Motion," J. Fluid Mech., 113, 347-386.

Koop, C.G. and B. McGee (1986), "Measurements of Internal Gravity Waves in a Continuously Stratified Shear Flow," J. Fluid Mech., 172, 453-480.

Lindzen, R.S. (1981), Turbulence and Stress Due to Gravity Wave and Tidal Breakdown," J. Geophys. Res., 86C, 9707-9714.

Maslowe, S.A. (1973), "Finite-Amplitude Kelvin-Helmholtz Billows," Bound-Layer Meteorol., 5, 43-52.

Maslowe, S.A. (1977), "Weakly Nonlinear Stability Theory of Stratified Shear Flows," Quart. J. Roy. Meteor. Soc., 103, 769-783.

Maslowe, S.A. (1986), "Critical Layers in Shear Flows," Ann. Rev. Fluid Mech., 18, 405-432.

Merrill, J.T. and J.R. Grant (1979), "A Gravity Wave-Critical Level Encounter Observed in the Atmosphere," J. Geophys. Res., 84, 6315-6320.

Orlanski, I. and K. Bryan (1969), "Formation of the Thermocline Step Structure by Large-Amplitude Internal Gravity Waves," J. Geophys. Res., 74, 6975-6983.

Plumb, R.A. and A.D. McEwan (1978), "The Instability of a Forced Standing Wave in a Viscous Stratified Fluid: A Laboratory Analogue of the Quasi-Biennial Oscillation," J. Atmos. Sci., 35, 1827-1839.

Scranton, D.R. and W.R. Lindberg (1983), "An Experimental Study of Entraining, Stress-Driven, Stratified Flow in an Annulus," Phys. Fluids, 26, 1198-1205.

Thorpe, S.A. (1968), "A Method of Producing a Shear Flow in a Stratified Fluid," J. Fluid Mech., 32, 693-704.

Thorpe, S.A. (1971), "Experiments on the Instability of Stratified Shear Flows: Miscible Fluids," J. Fluid Mech., 46, 299-319.

Thorpe, S.A. (1973), "Turbulence in Stably Stratified Fluids: A Review of Laboratory Experiments," Boundary-Layer Meteorol., 5, 95-119.

Thorpe, S.A. (1981), "An Experimental Study of Critical Layers," J. Fluid Mech., 103, 321-344.

Wallace, J.M. and V.E. Kousky (1968), "Observational Evidence of Kelvin Waves in the Tropical Stratosphere," J. Atmos. Sci., 25, 900-907.

FIGURE CAPTIONS

1. The experimental facility. The side view shows one of 32 piston assemblies.

2. Measured density profiles. The dashed line was obtained before the lid started; the solid line was taken at the end of the experiment. Z is height above the bottom floor. Z_{max} is the total water depth of 38.7 cm.

3. The velocity profile at the start of the experiment. Circles (squares) are from a 4-second (1-second) exposure photograph. The solid line (dashed line) is a subjective fit (exponential fit) to the data.

4. Schematic drawing of early wavebreaking. Arrows indicate the direction of the rolling motions.

5. Five shadowgraph images of early wavebreaking. The bottom floor is started at 0:00. The times of the photographs are (a) 2:22, (b) 3:11, (c) 3:54, (d) 4:07, and (e) 6:55. The area shown is approximately 36 cm wide by 12 cm high. The right-hand scale is 2.5 cm between tic marks. The arrow on each scale denotes the depth of $Z/Z_{max} = 0.59$. The photographs are taken at different phases of the forced wave. The stipled region in each photograph

covers the reflection of the shadowgraph light source from the side walls of the tank.

6. One-second exposure streak photograph showing rolling motions at a depth just above the clock. The background grid is 10-cm square.

7. Schematic drawing of the late-time mixing regions. Arrows indicate the direction of the rolling motions.

8. Instantaneous velocity profile from a streak photograph around t = 5:00. The solid line is a subjective fit through the data; the dashed line is the initial profile from Figure 3.

9. Four instantaneous velocity profiles taken every quarter of a wave period during one wave cycle around t = 5:00 (thin solid lines). The heavy dark line is the mean velocity profile. The dashed line is the initial profile from Figure 3.

10. Evolution of the mean velocity profile with time. Times are in minutes after starting the bottom floor.

11. Instantaneous particle velocities at times of (a) 5, (b) 10, (c) 20, and (d) 75 minutes after starting the bottom floor. The dashed line indicates the phase speed of the forced wave. Arrows indicate the depths over which wavebreaking was observed from the shadowgraph.

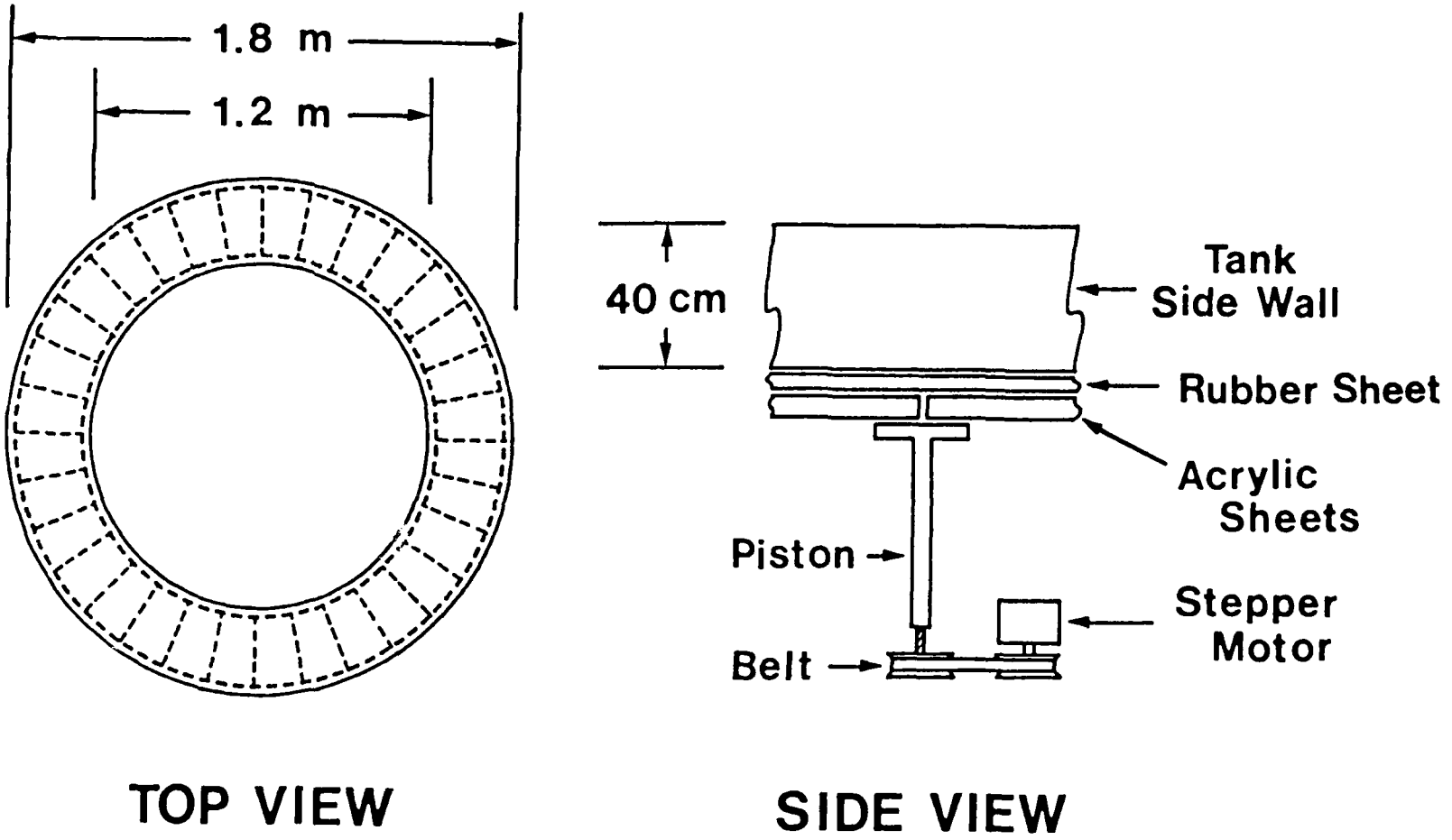
1.8 m
1.2 m
40 cm
Tank
Side Wall
Rubber Sheet
Acrylic
Sheets
Piston
Stepper
Motor
Belt
TOP VIEW
SIDE VIEW

Figure 1.

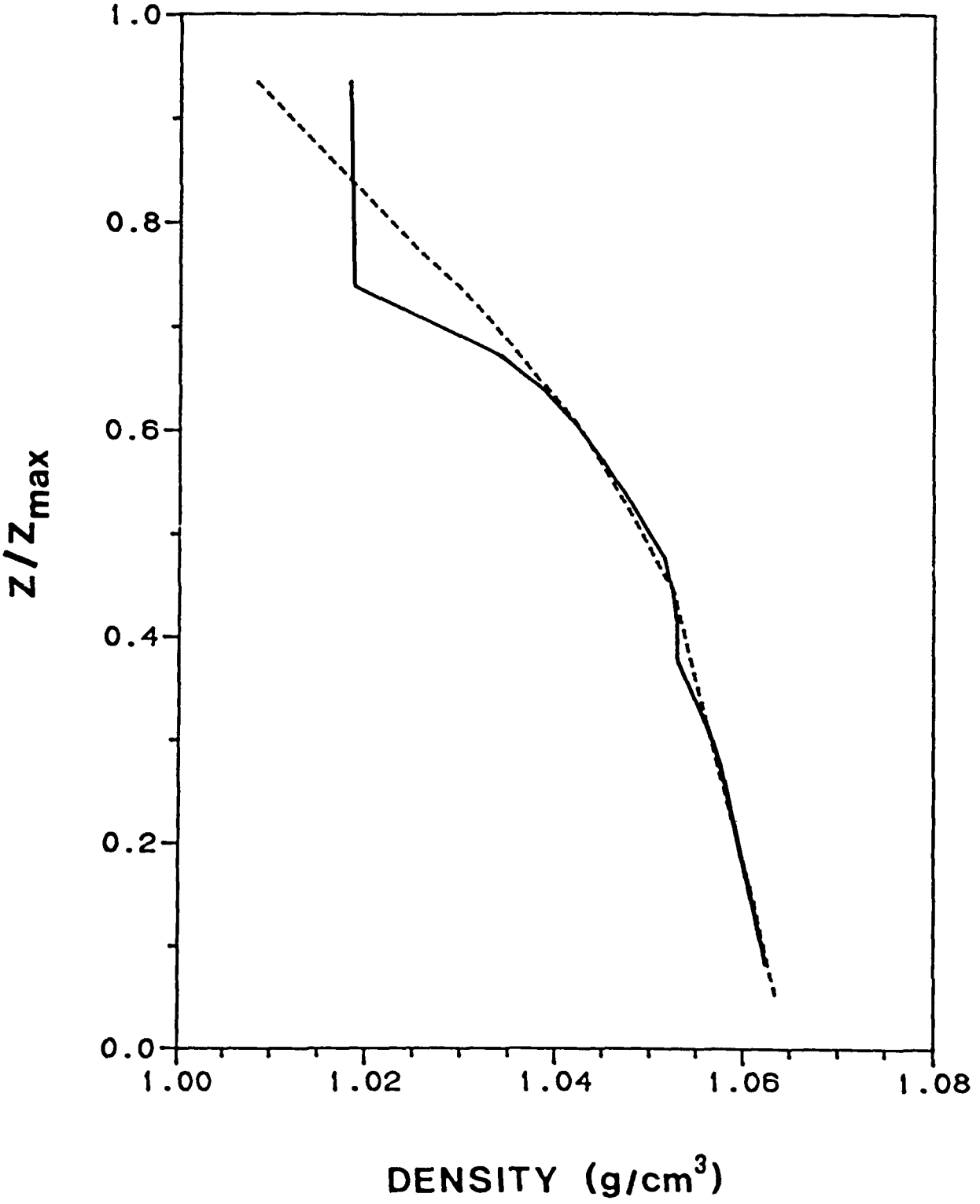

Figure 2.

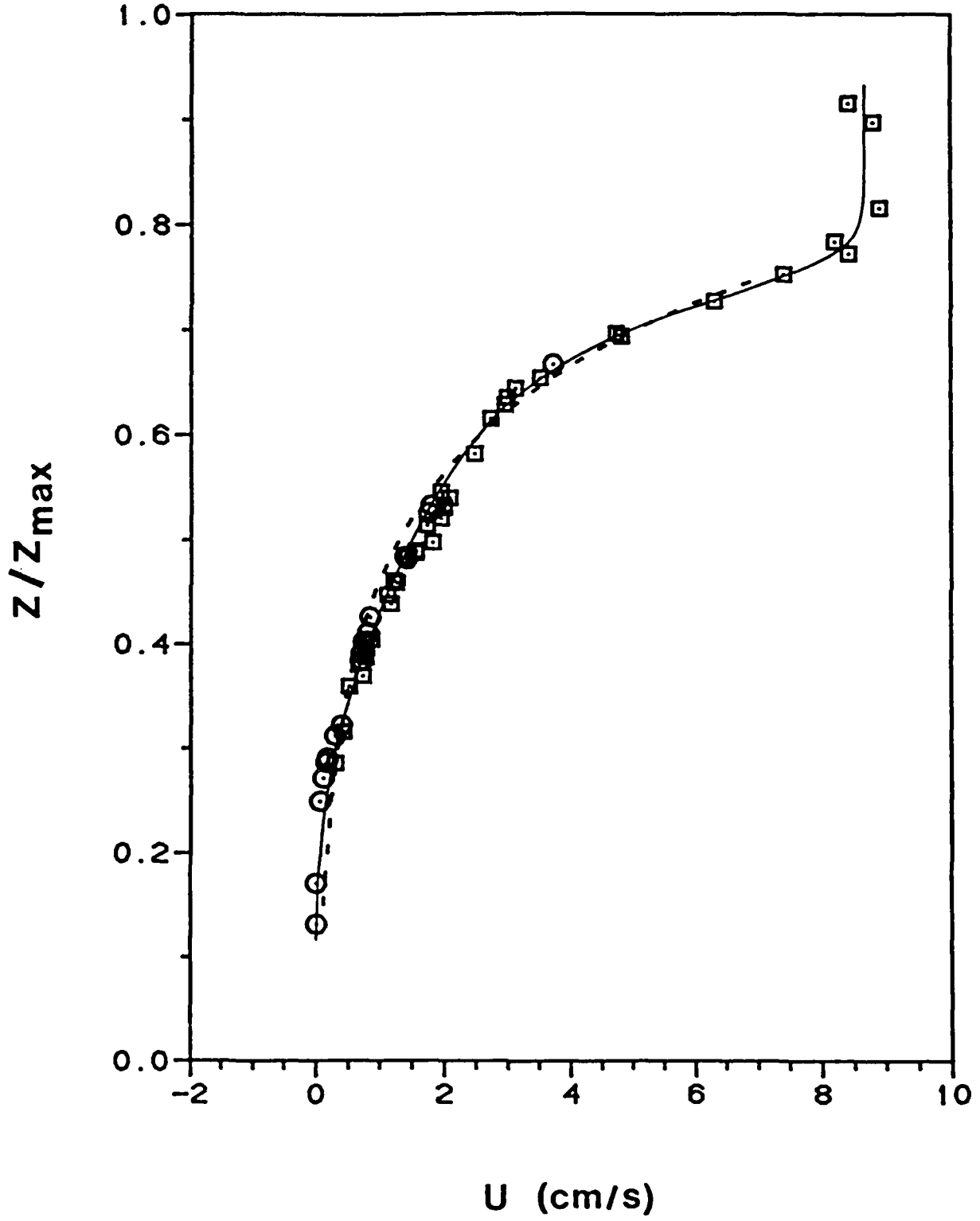

Figure 3.

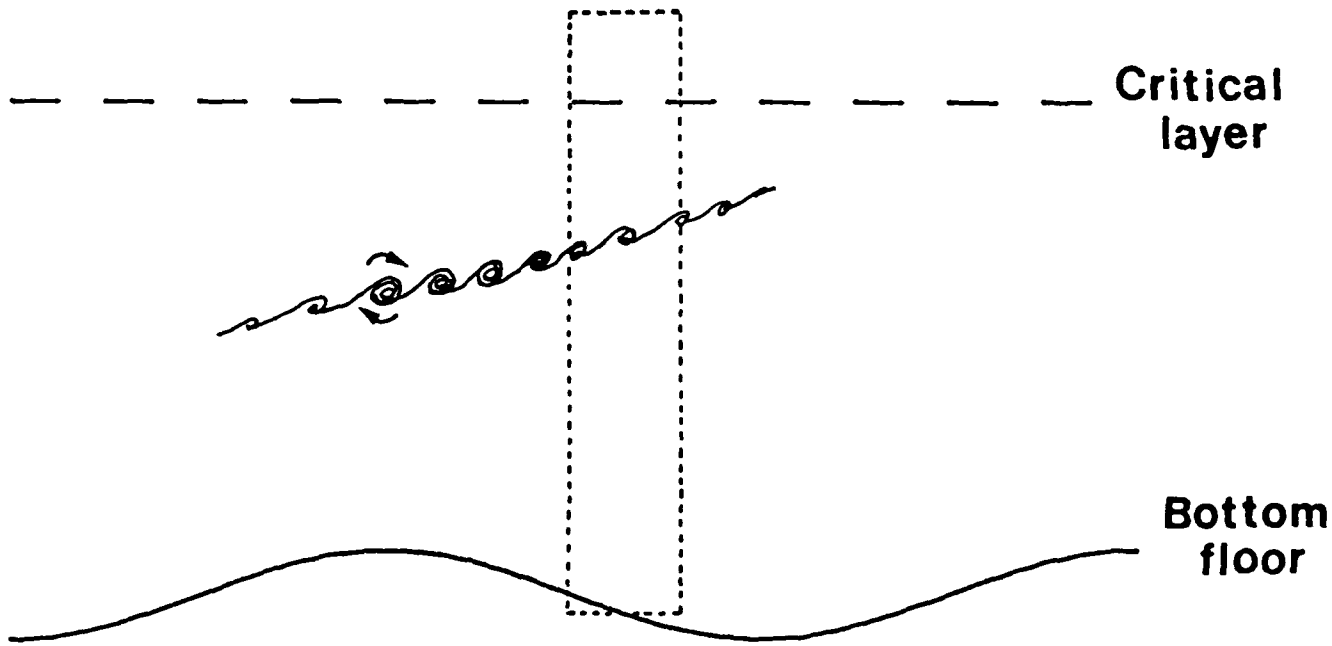

Figure 4.

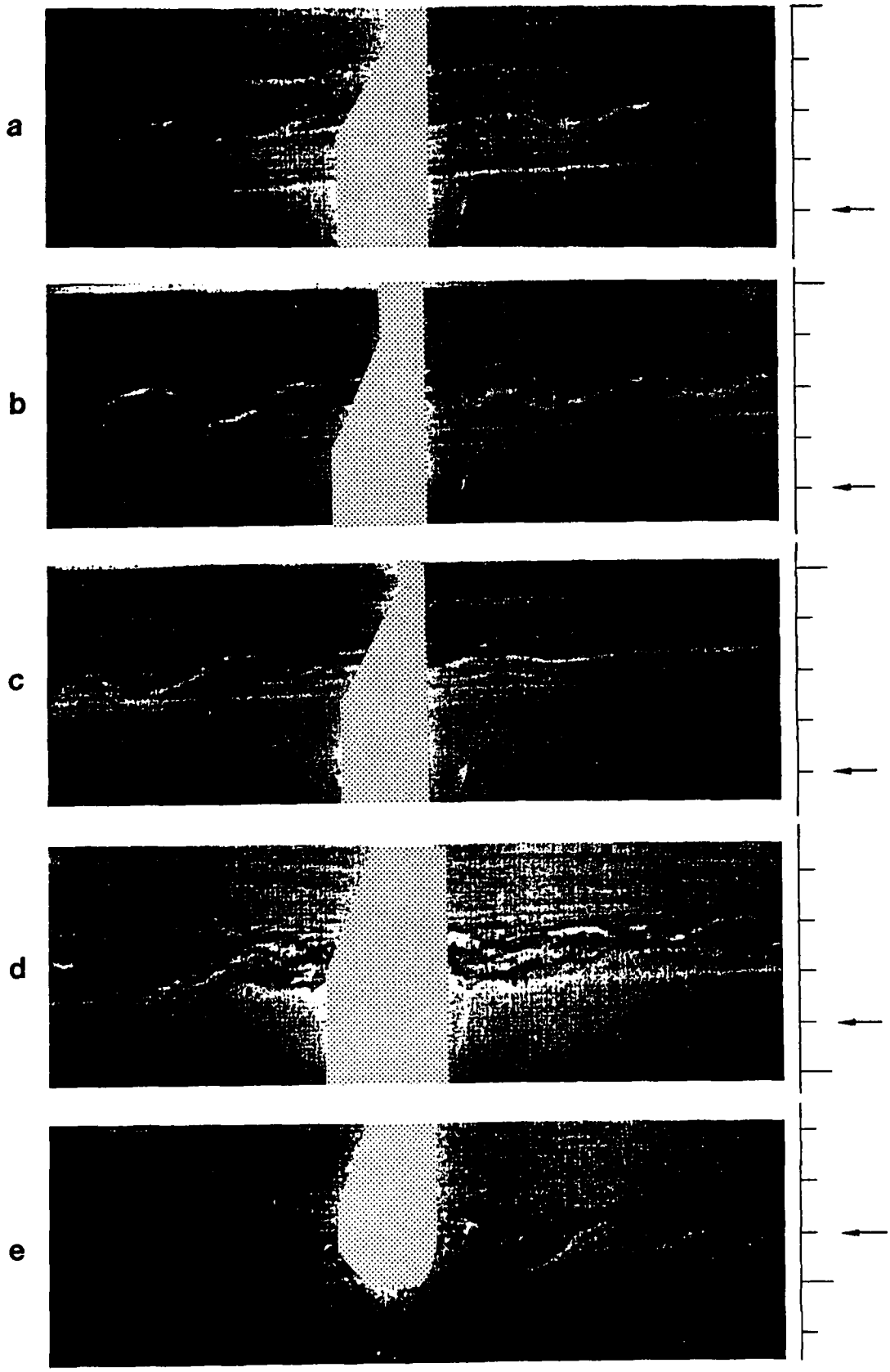

Figure 5

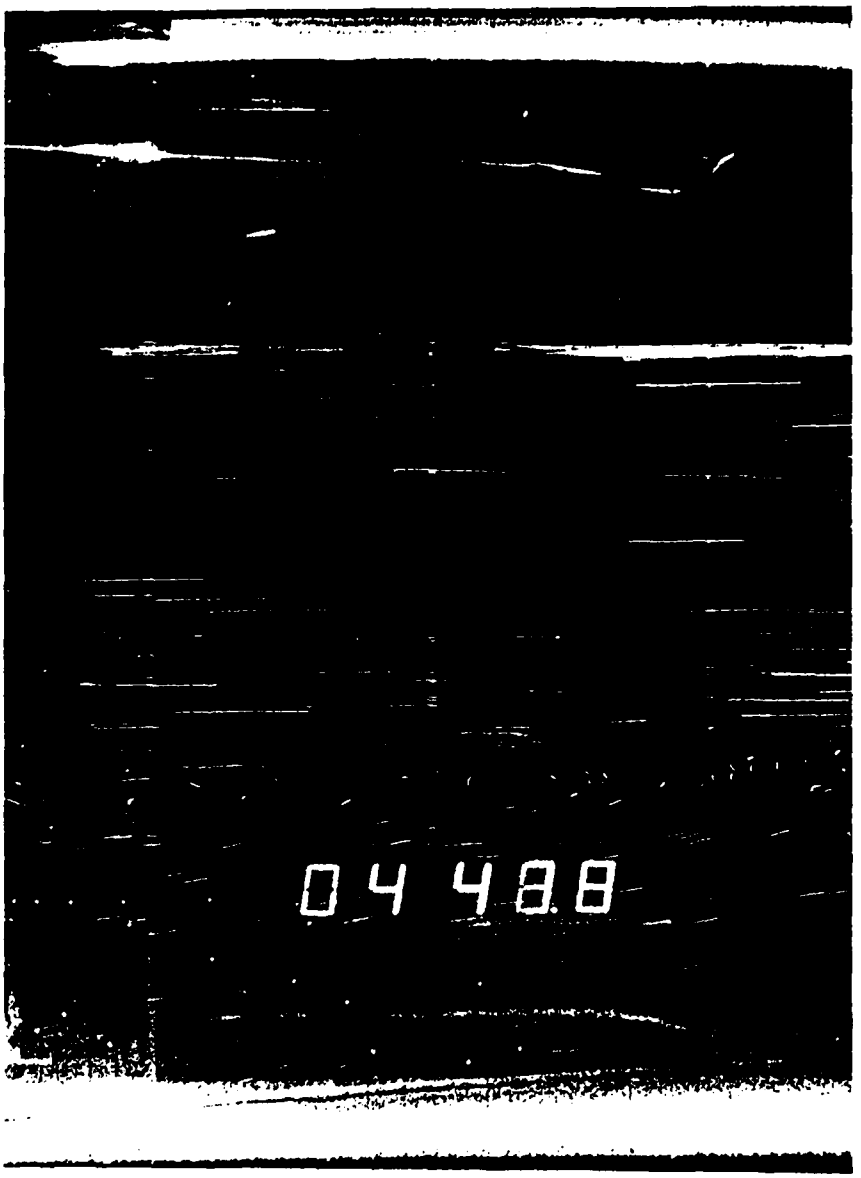

Figure 6

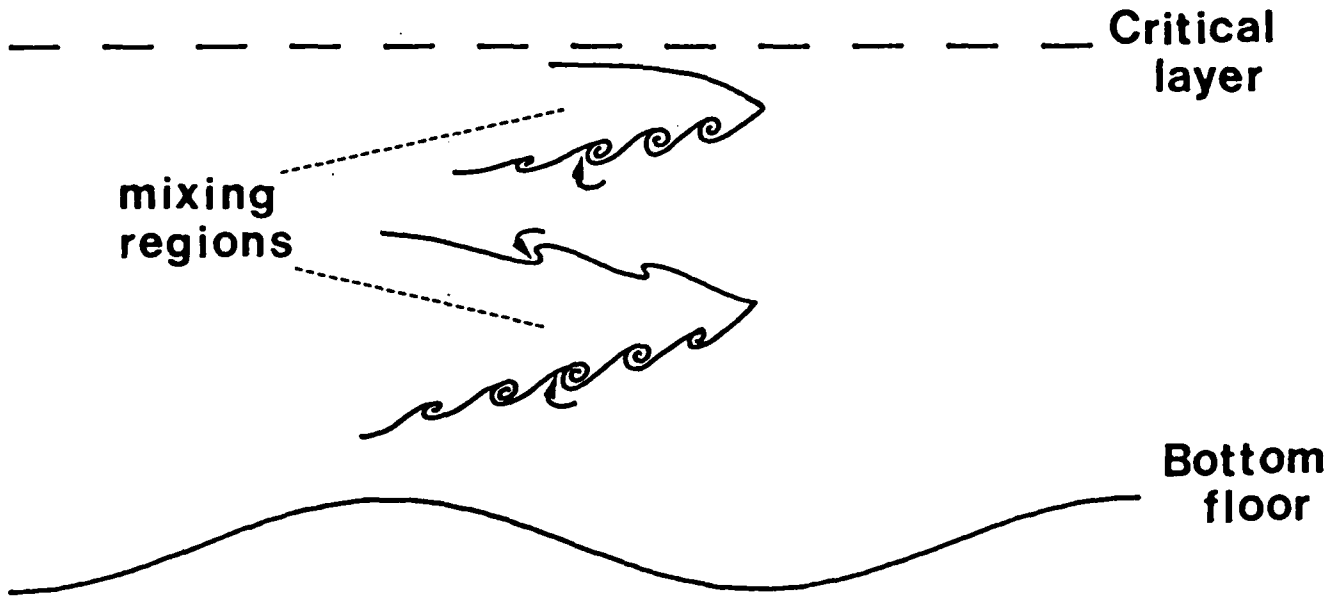

Figure 7.

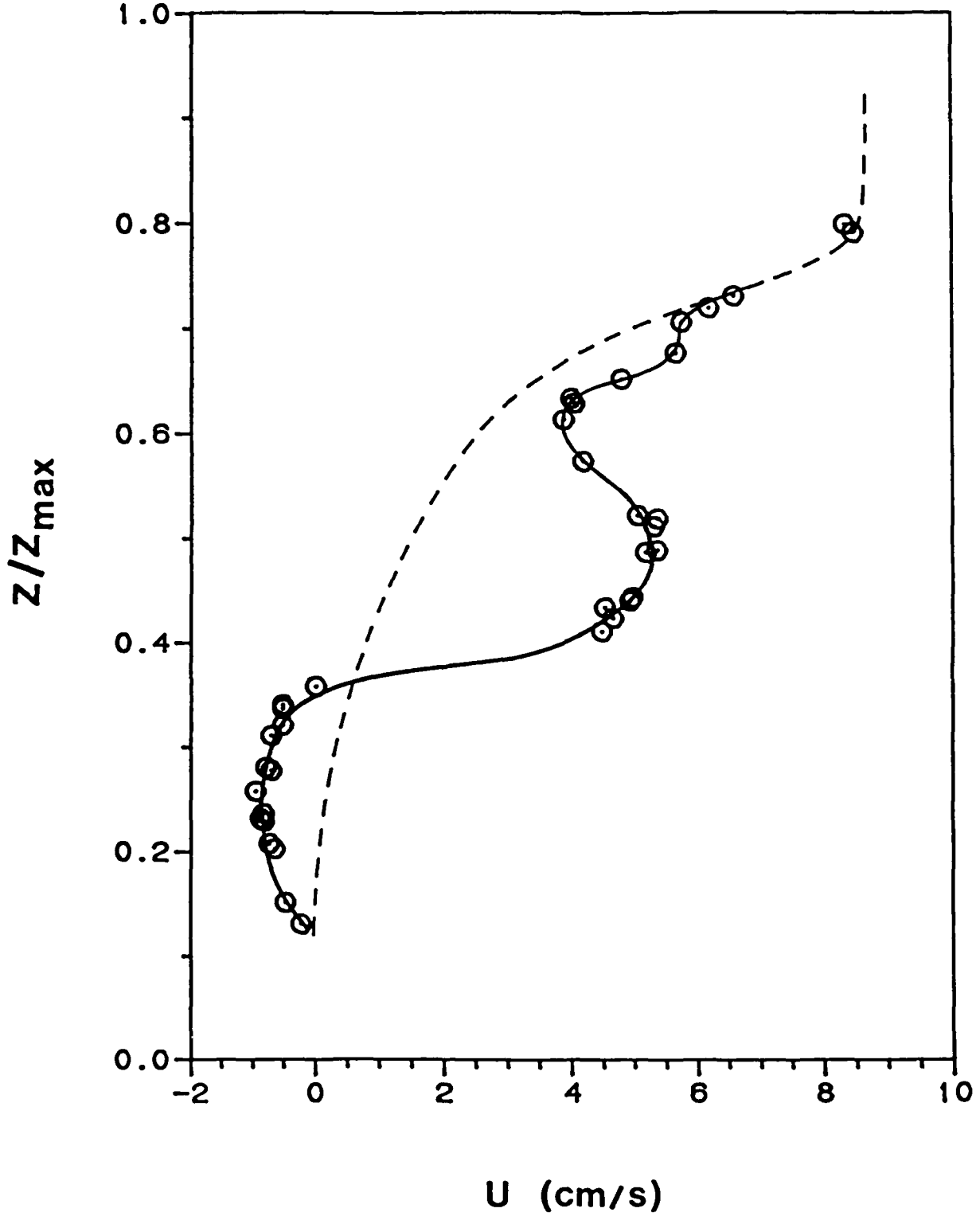

Figure 8.

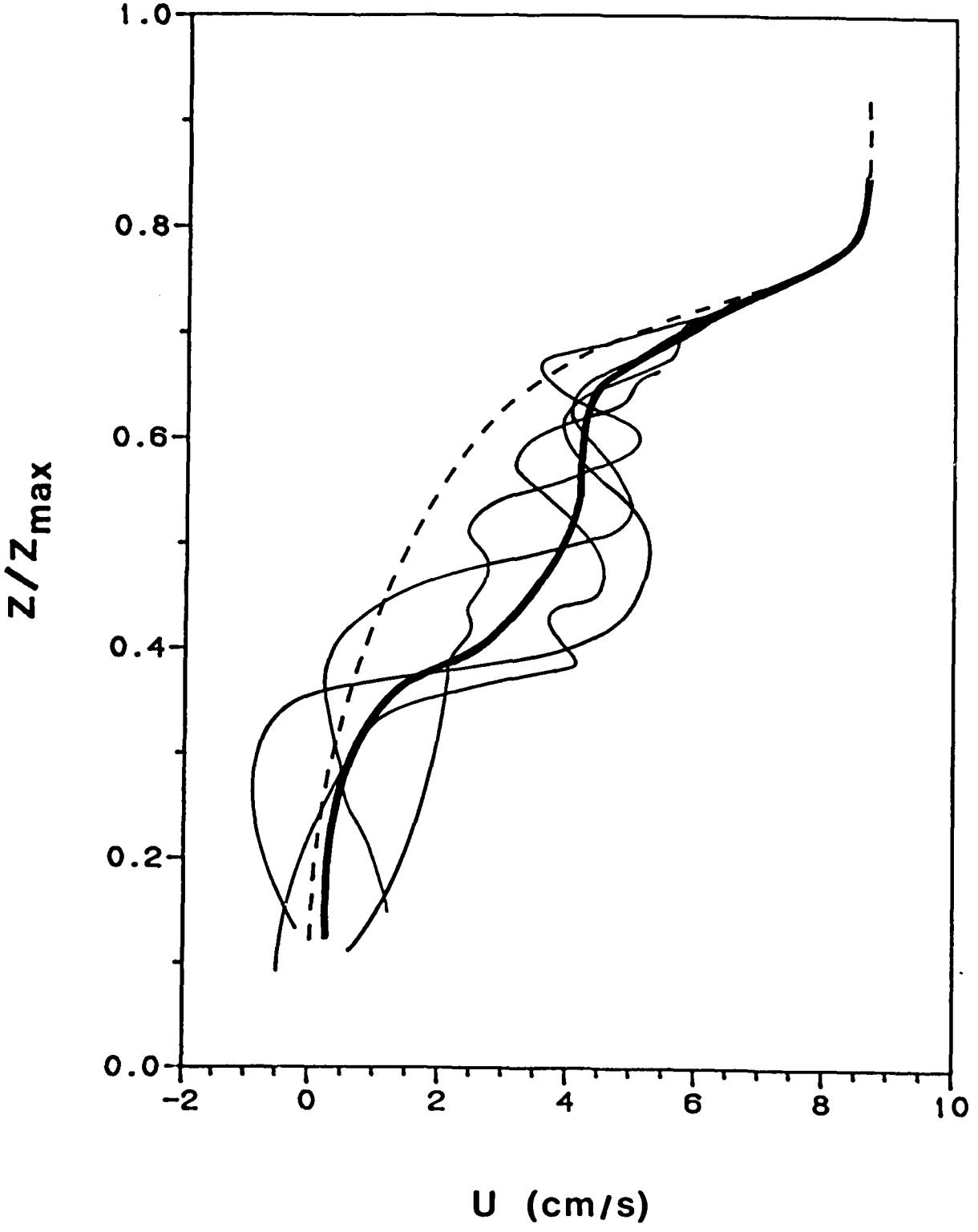

Figure 9.

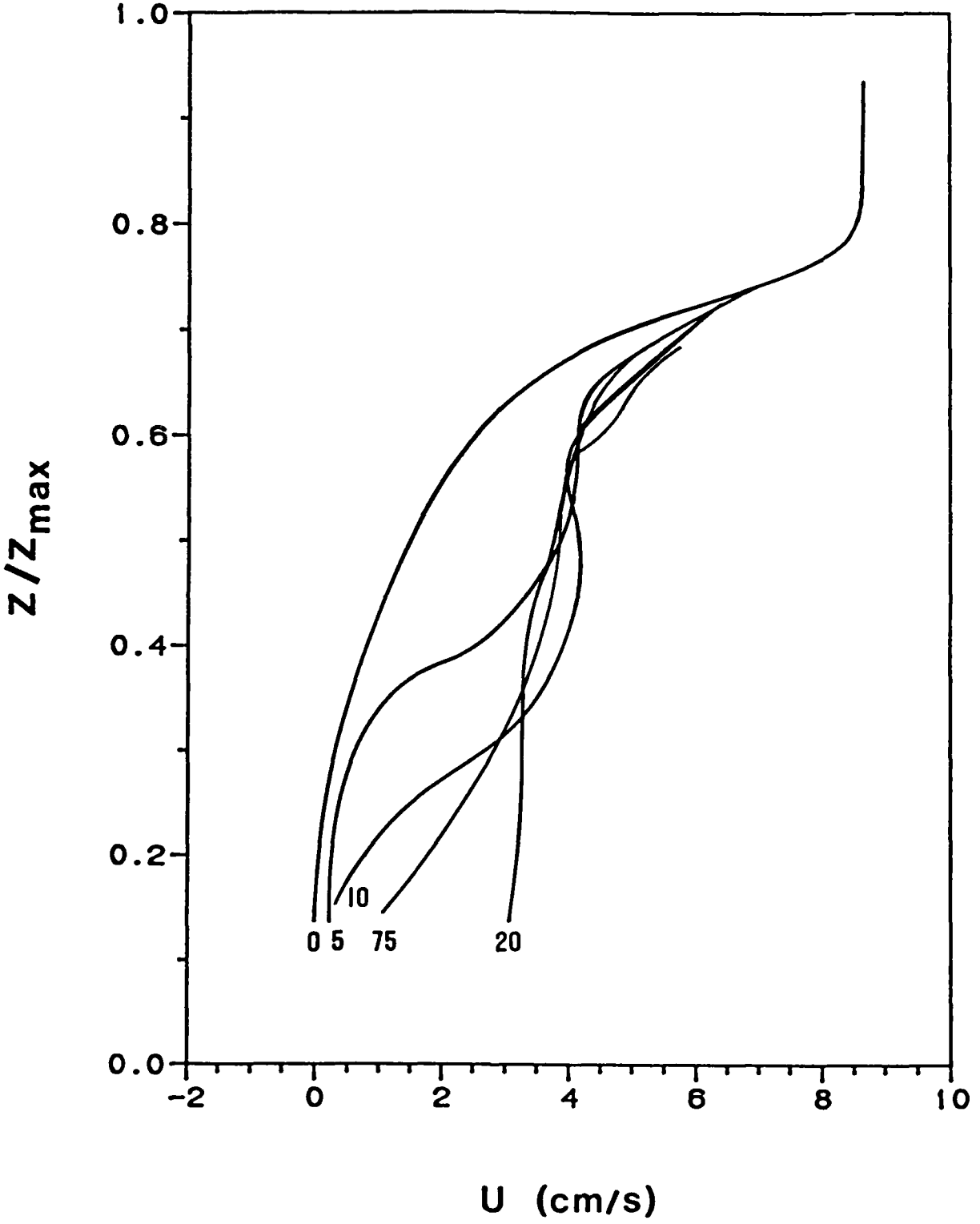

Figure 10.

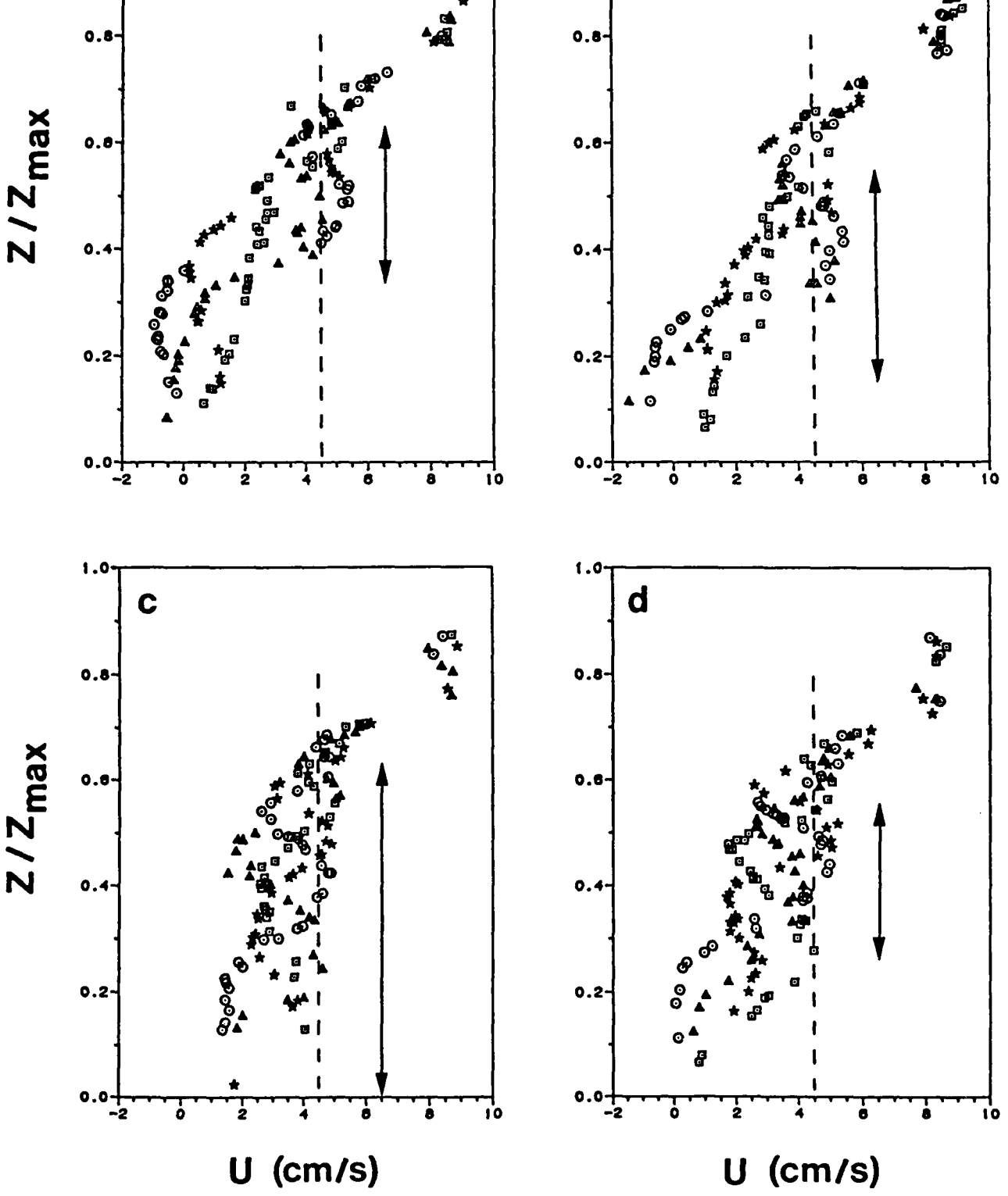

Figure 11.